Wetting and emergence of long-range couplings in arrays of fluid cells

D. B. Abraham,[1] A. Maciołek ◉,[2,3,*] and A. Squarcini ◉[4]

[1]*Rudolf Peierls Centre for Theoretical Physics, University of Oxford, Clarendon Laboratory, Oxford OX1 3PU, United Kindgom*
[2]*Institute of Physical Chemistry, Polish Academy of Sciences, PL-01-224 Warsaw, Poland*
[3]*Max-Planck-Institut für Intelligente Systeme, D-70569 Stuttgart, Germany*
[4]*Institut für Theoretische Physik, Universität Innsbruck, A-6020 Innsbruck, Austria*

Critical wetting is of crucial importance for the phase behavior of a simple fluid or Ising magnet confined between walls that exert opposing surface fields so that one wall favors liquid (spin up), while the other favors gas (spin down). We show that arrays of boxes filled with fluid and linked by channels with appropriately chosen opposing walls can exhibit long-range cooperative effects on a length scale far exceeding the bulk correlation length. We give the theoretical foundations of these long-range couplings by using a lattice gas (Ising model) description of a system.

I. INTRODUCTION

Correlation effects occurring over large distances are of great interest in condensed-matter physics from both fundamental and practical viewpoints. In a series of experiments, Gasparini and coworkers [1,2] observed the emergence of long-range couplings in arrangements of bulklike regions of near-superfluid ^{4}He. These experiments involve planar arrays of micrometer-sized cells etched in a Si wafer filled with near-superfluid ^{4}He and connected either through a supernatant nanoscopic ^{4}He layer or via shallow channels. Remarkably, even though the boxes had a mesoscopic spacing, various measurements showed clear evidence of coupling between different boxes extending over distances much larger. than the bulk correlation length. This cooperative phenomenon, subsequently termed action at a distance (AAAD) by M. E. Fisher [3], was attributed to proximity effects induced by cell and channel size, as well as proximity to the critical point. The authors of Ref. [1] made an interesting suggestion that AAAD effects of this type might be a more general feature of systems with phase transitions, both quantum (like ^{4}He) and classical.

Intrigued by these suggestions, we presented a theoretical model of a classical system exhibiting correlation effects which are similar to the ones observed in superfluid helium [4,5]. This model comprises boxes—cubic or square Ising lattices of a finite size—arranged in a two-dimensional (2D) array and coupled together by Ising strips. We have shown that with appropriately tuned temperature and size of array

components, a lattice of boxes develops long-range order even though the connecting strips are very long compared to their lateral dimensions, as in the case of the arrangement considered by Gasparini and coauthors. We have argued that the same applies when cubes are connected by rods. Monte Carlo simulations confirmed these predictions and provided thermodynamic data, which signal the emergence of the long-range order. Physical realizations of our model include uniaxial classical ferromagnets or simple fluids and binary mixtures in the lattice gas approximation (all belonging to the Ising model universality class of critical phenomena in contrast to the superfluid ^{4}He, which belongs to the universality class of XY model).

In Refs. [4,5] we imposed free boundary conditions on the boxes and the channels (strips or rods) connecting them. Although free boundary conditions are natural for quantum fluids such as ^{4}He, because the superfluid order parameter (the phase of the wave function) does not couple to the cells boundaries, they are rather unusual for classical fluids. Typically, the molecules of the fluid are attracted to the boundaries of a container, which causes the density of the fluid near the boundaries to increase and leads to adsorption and wetting phenomena [6]. In terms of a lattice-gas description this corresponds to the presence of a (dimensionless) surface field h_1. For binary liquid mixtures one has $h_1 \sim \delta \Delta \mu_1 / k_B T$, where $\delta \Delta \mu_1$ is a local increment at the boundaries of the chemical potential difference between the two components of the mixture [7]. It determines which component of the binary mixture is preferred at the boundaries. The preference for one component of a binary liquid mixture may be so strong as to saturate the boundary of container with the preferred component, which corresponds to $h_1 = +\infty(-\infty)$. If neither component is preferred, then we have $h_1 = 0$. At this point, it is natural to ask how sensitive the AAAD phenomenon is to modifications of boundary conditions to take surface fields into account. For free boundary conditions, it is the state of the connecting channel that determines the long-range coupling
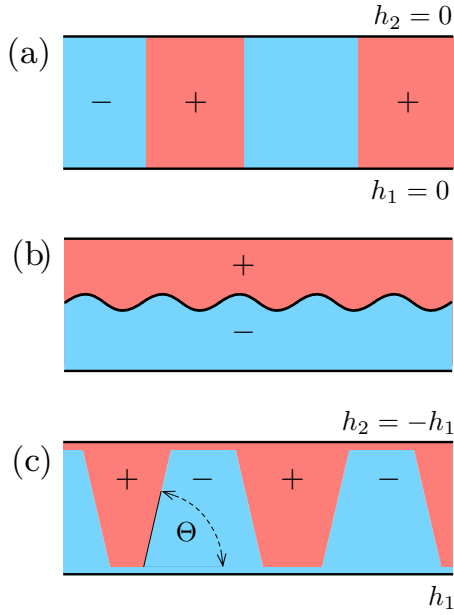
*maciolek@is.mpg.de

FIG. 1. Domain walls, by which we mean Peierls contours after summing out fluctuations up to a scale of the bulk correlation length, in a strip (a) with free boundary conditions below the critical temperature T_c, (b) with opposing infinite surface fields $h_1 = -h_2 = \infty$ below T_c, and (c) with finite opposing surface fields corresponding to weakened surface bonds below the wetting temperature $T_w(h_1) < T_c$.

between boxes. Below the critical temperature T_c, while the state of each large box is either magnetized positively or negatively, the dominant spin configurations in the Ising strip involve Peierls contours [8,9] separating regions of alternating $(+)$ and $(-)$ magnetization that terminate at the edges of the strip, as sketched in Fig. 1(a). [It is clear that closed Peierls contours are allowed in the form of bubbles of phase $(-)$ in the cluster of phase $(+)$ and vice versa.] These Peierls contours are responsible for breaking up long-range order in the channel on the characteristic length scale, which emerges from asymptotic spectral degeneracy in transfer matrices [10,11] and which is much larger than the bulk correlation length. The existence of such a characteristic length scale is intimately related to the appearance of the long-range order in 2D arrays. In the case of Ising strips or rods with all boundary spins equal to $+1$, or more generally, if surface fields at the edges have the same sign $(h_1 h_2 > 0)$, then there is no asymptotic spectral degeneracy in transfer matrices [12–14] and hence no long-range cooperative effects in 2D arrays. In the presence of equal and opposite surface fields $h_1 = -h_2$, such degeneracy appears in the partial wetting regime [14]. However, the mechanism of asymptotic degeneracy in this case is quite different from the mechanism in the strip with free edges. For strips with equal and opposite surface fields, the boundaries are covered with the $(+)$ or $(-)$ phase, and below T_c there is a *single* open Peierls contour separating these two regions of opposite magnetization [15]. For infinite surface fields $h_1 = -h_2 = +\infty$, the Peierls contour, entropically repelled from both boundaries, maximizes its distance from them by fluctuating in the middle of the strip, as depicted in Fig. 1(b); there are no asymptotically degenerate states in that case. However, for finite surface fields corresponding to

weakened surface bonds, there is a temperature range where the Peierls contour runs close to the boundary, but since the surface fields have the same strength, it switches back from one side of the strip to the other, as shown in Fig. 1(c). This switching occurs below the single-wall wetting temperature $T_w(h_1) < T_c$ and is caused by asymptotic degeneracy, which can be explained by the concept of surface states, as we will show in this paper. The presence of asymptotically degenerate states in the connecting channels means that long-range effects can be expected in systems of boxes connected by strips with appropriately selected equal and opposite surface fields. This would open an intriguing possibility of tunability not only for uniaxial classical ferromagnets but also for fluid systems and could be used, e.g., in as a microfabricated device in soft-matter and biophysics experiments.

Here we explore this possibility by using a mesoscopic description, which is in the spirit of Fisher-Privman theory of finite-size effects at first-order transitions [16] and which gives a simple physical picture of a typical spin configuration in a channel below the wetting temperature. By applying this description we reduce the problem to a "network" planar Ising model that focuses on the state of the cubes. For large-enough cubes, the state of each cube is characterized by $+1$ and -1 magnetization. These "boxes" are coupled by channels in which the internal degrees of freedom have been summed out, producing an Ising superlattice of nodes with the effective coupling that are temperature dependent. In the case of 2D channels, we extend our mesoscopic description utilizing exact results for the full Ising strip. This allows us to make a quantitative prediction of the temperature range and the size of the connecting strips for which the "network" develops long-range order.

The paper is organized as follows. First, we show that in Ising strips with "wetting boundaries," i.e., with finite opposing surface fields $h_1 = -h_2$ corresponding to weakened surface bonds, a characteristic divergent length scale $\xi_\parallel$ develops below the wetting temperature $T_w(h_1)$. This can be inferred, e.g., from the decay of the spin-spin correlation function. In Sec. II we demonstrate that the spin-spin correlation function can be obtained from coarse-grained description if one takes into account that in a partial wetting regime a typical spin configuration is one with domain walls inclined at the contact angle Θ to the edge of the strip [see Fig. 1(c)] [17]. We derive the contact angle Θ and the statistical weight of such an inclined domain wall in an independent exact calculation in the Ising strip with surface fields (Appendices A and D). In addition to the contribution due to the angle-dependent surface tension, this statistical (Boltzmann) weight includes a term due to point tension τ_p [18]; the latter is the 2D equivalent of line tension in 3D [6]. We show that τ_p diverges logarithmically on approaching the wetting. In Sec. III we construct the "network" planar Ising model and find the range of parameters for which it develops long-range order. For comparison with the coarse-grained theory presented in Sec. II, in Sec. IV we calculate the spin-spin correlation function for Ising strips with surface fields exactly using the transfer matrix method. In particular, we demonstrate how for wetting boundaries below $T_w(h_1)$ the ferromagnetic order is attained over distances of the order of characteristic length scale $\xi_\parallel$ that diverges exponentially with the cross section of the channels. We show

that $\xi_\parallel$ emerges as the inverse mass gap between two asymptotically degenerate modes in the spectrum of the transfer matrix. Our approach allows us to treat the case of opposite surface fields $(h_1 h_2 < 0)$ in contrast to the technique used by Au-Yang and Fisher [19] which is only applicable to the case of $h_1 h_2 > 0$. Moreover, we construct surface states corresponding to two phases pseudocoexisting in the partial wetting regime $T < T_w(h_1)$. Note that for bulk 2D systems there can be no true phase transition in the strip geometry. However, there is still a line of sharp (very weakly rounded) first-order phase transitions ending in the pseudocritical point [16,20]. Our conclusions are summarized in Sec. V.

II. STRIPS WITH OPPOSING SURFACE FIELDS: MESOSCOPIC DESCRIPTION

We start by considering the phase behavior of connecting channels with surface fields at the boundaries. For a 2D Ising strip with wetting boundaries $h_1 = -h_2$, at low temperatures one finds pseudocoexistence at zero bulk field, where large domains of the "bulk" phases are formed [21–24]. In this respect, the asymmetric strip behaves in the same fashion as the strip with free boundaries $h_1 = -h_2 = 0$. At higher temperatures the influence of wetting manifests itself. For the semi-infinite square Ising model with a surface field h_1 Abraham's [25] exact solution shows that for a range of h_1 there is a critical wetting transition at a strictly subcritical temperature given by $w = 1$ with

$$w = e^{2K_1}(\cosh 2K_2 - \cosh 2h_1)/\sinh 2K_2, \qquad (1)$$

and $0 < h_1 < K_2$; $K_1 = \beta J_1$ and $K_2 = \beta J_2$ are the coupling constants of interactions along bonds perpendicular and parallel to the surface, respectively. In the region $w > 1$, the interface is found on average at a finite distance from the wall, i.e., it is pinned. Above the transition, the interface depins to a fluctuating regime. In considering asymmetric strips it means that by choosing h_1 one can tune the temperature region of pseudocoexistence, where large domains exhibiting thin "wetting" films exist. For example, if h_1 is weak, then pseudocoexistence occurs almost all way up to the bulk critical temperature T_c. The same scenario should apply to the cubic Ising model in slab and rod geometry [20,26–28].

On the scale of bulk correlation length, a typical configuration at pseudocoexistence is one with regions of alternating $(+)$ and $(-)$ magnetization, with a magnitude roughly the spontaneous magnetization, separated by domain walls. Unlike a strip with free boundaries, where domain walls run perpendicular to the edges to minimize an energetic penalty proportional to their length, in a strip with surface fields they are inclined at the contact angle $\Theta(h_1, T)$ as shown in Fig. 2. The exact expression for the contact angle is [17]

$$\tan \Theta = \frac{w^2 - 1}{[(A - w)(B - w)(w - A^{-1})(w - B^{-1})]^{1/2}}. \qquad (2)$$

Figure 3 shows Θ as function of the variables h_1 and T. The derivation of $\Theta(h_1, T)$ is carried out in Appendix A, and there the meaning of the notation for A and B is explained.

As first pointed out by Parry and Evans [23,24], the characteristic length $\xi_\parallel$ of successive domains of $(+)$ and $(-)$ magnetization in the nonwet regime should diverge
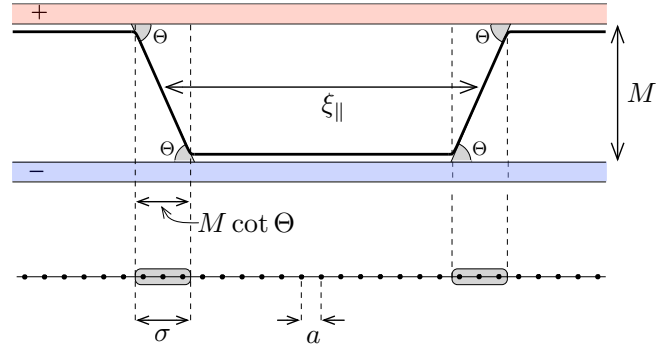

FIG. 2. A configuration of domain walls in the channel with wetting boundaries. Domain walls form a contact angle Θ with the solid wall and $\xi_\parallel$ provides a measure of their separation. The effective picture is that of one-dimensional lattice gas of particles with diameter $\sigma = 1 + [M \cot \Theta]$.

exponentially with the width of the strip. This prediction is consistent with exact results from the restricted solid-on-solid model of an interface, where $\xi_\parallel$ is obtained from the two largest eigenvalues of the transfer matrix [29,30]. In Sec. IV C we show that for 2D Ising strips the exact result for $\xi_\parallel$ is

$$\xi_\parallel = \frac{(Aw - 1)(Bw - 1)}{2w\sqrt{AB}(w - w^{-1})^2} w^M; \qquad (3)$$

the exponential growth follows from $w > 1$.

The exponential divergence of $\xi_\parallel$ can also be inferred in a simple way by using a coarse-grained description based on domain walls. To this end, we treat the collection of domain walls for the strip geometry as a quasi-one-dimensional gas of strictly avoiding particles on a lattice. To account for the slope of the domain wall, we assume that the particles are not pointlike but have a diameter σ. The domain-wall projection onto the edge of the strip is equal to $M \cot \Theta$ as shown in
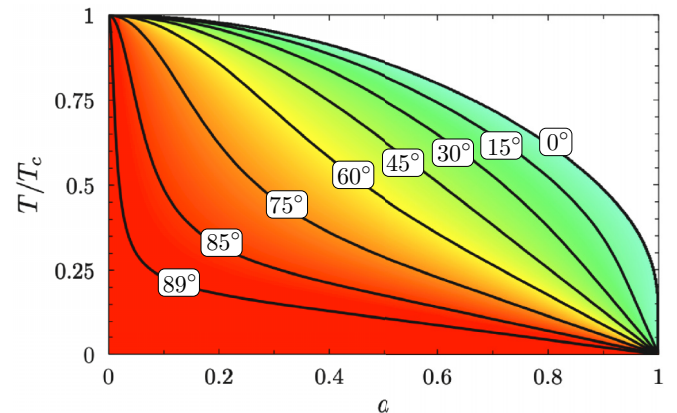

FIG. 3. The contact angle Θ as function of the rescaled field $a = |h_1|/K_2$ and temperature T; the solid black lines indicate the contour lines of constant contact angle Θ. The locus with $\Theta = 0$ corresponds to the wetted phase boundary where $w(h_1, T) = 1$. The contact angle tends to $\pi/2$ for any subcritical temperature provided the surface field tends to zero; therefore for free boundaries $\Theta(h_1 = 0, T) = \pi/2$, and domain walls are perpendicular to the strip edges. In this figure $K_1 = K_2$.

Fig. 2. On a lattice with the lattice constant $a = 1$ we set $\sigma = [M \cot \Theta] + 1$, where the symbol $[x]$ denotes the integer part of x, i.e., x is the greatest integer less than or equal to x. If the surface fields vanish, then $\sigma = a$ so the domain wall becomes a pointlike particle, which is the case we studied in Refs. [4,5].

The equilibrium statistical mechanics of this system can be determined within the grand-canonical ensemble. If $\widetilde{\zeta}$ is the fugacity corresponding to the Boltzmann weight associated with an isolated domain wall, then the grand partition function for a strip of length L is

$$\Xi^{\text{rods}}(\widetilde{\zeta}, L, \sigma) = \sum_{j=0}^{[L/\sigma]} \binom{L - j\sigma + j}{j} \widetilde{\zeta}^{j}, \qquad (4)$$

where $[L/\sigma]$ is the maximum number of particles that can be allocated on the strip of length L. The binomial coefficient counts all possible arrangements of j indistinguishable hard rods of length σ on a lattice of length L. The rods are hard in the sense that they can touch but not overlap. For free boundary conditions the diameter becomes a lattice unit, and then the combinatorial factor in Eq. (4) reduces to the binomial $\binom{L}{j}$ [31].

For any $\sigma \geqslant 2$ and for arbitrary $\widetilde{\zeta}$ the grand partition function can be expressed in terms of generalized hypergeometric functions. Since the distance between the domain walls is large, we can approximate the grand partition function Ξ^{rods} by reducing the problem of hard rods on a lattice to the one of point particles on a coarse lattice with a lattice constant of σ. In fact, the problem is reduced to the study of the diluted limit of a hard rod gas. (For a formal details of this approximation as well as the connection to the continuum version of the model known as the Tonks-Rayleigh hard rod gas [32,33], see Appendix B.) This approximation gives

$$\Xi^{\text{rods}}(\widetilde{\zeta}, L, \sigma) \approx \sum_{j=0}^{\ell} \binom{\ell}{j} \sigma^{j} \widetilde{\zeta}^{j} = (1 + \widehat{\zeta})^{\ell}, \qquad (5)$$

where $\widehat{\zeta} = \sigma \widetilde{\zeta}$ and $\ell = L/\sigma$.

Within this simple physical picture, the calculation of the pair correlation function $G(x)$ for a separation $x = \sigma n$ is straightforward. If a pair of spins is parallel (antiparallel), then they are separated by an even (odd) number of domain walls. Denoting by $\Xi_e(x)$ and $\Xi_o(x)$ the grand partition function with an even and odd number of particles, respectively, we find

$$G(x) \propto \frac{\Xi_e(x) - \Xi_o(x)}{\Xi_e(x) + \Xi_o(x)} = \frac{(1 - \widehat{\zeta})^n}{(1 + \widehat{\zeta})^n}. \qquad (6)$$

The proportionality factor is not obtainable within this approach since on the mesoscopic scale, the local magnetization at the correlated sites is not ± 1. For $\widetilde{\zeta} \ll 1$, the expression for $G(x)$ can be simplified giving a purely exponential decay,

$$G(x) \sim G_0 \exp\{-2x\widetilde{\zeta}[1 + O(\widetilde{\zeta}^2)]\}. \qquad (7)$$

From the above expression it follows that the emerging parallel correlation length is

$$\xi_{\parallel} = 1/(2\widetilde{\zeta}). \qquad (8)$$

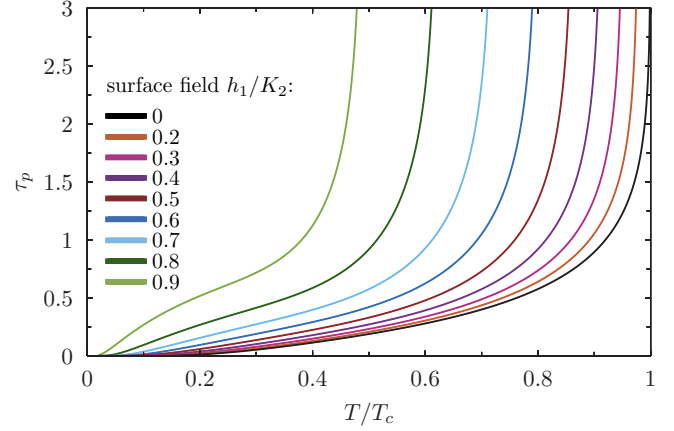This is consistent with Landau's argument about the lack of long-range order in a one-dimensional system with short-

FIG. 4. The point tension τ_p as function of temperature T for various surface fields (as shown in the inset). The rightmost curve (black) corresponds to the free edges $a = 0$. The point tension diverges logarithmically at the wetting temperature $T_w(h_1)$. In this figure, $K_1 = K_2$.

range interactions [34]. The statistical weight of a domain wall is taken *a priori* to be $\widetilde{\zeta} = \exp[-\mathcal{F}(\Theta)]$, where $\mathcal{F}(\Theta)$ is the energy cost associated with the insertion of a domain wall into the strip with opposing surface fields. This energy cost is proportional to M; hence, the mesoscopic description predicts that the decay length of the correlation function $G(x)$ *diverges exponentially with M*. In Appendices A and D we argue that $\mathcal{F}(\Theta) = Mv_0$ with $Mv_0 = M \csc \Theta \, \tau(\Theta) - M \cot \Theta f_0$, where $\tau(\Theta)$ is the angle-dependent surface tension [35,36] for an inclined interface forming a tilt angle Θ with the wall and f_0 is the surface free energy of a flat interface pinned to the wall.

We now compare this prediction with the results of exact calculations for the full Ising strip, which we present in Sec. IV. We find agreement in the asymptotic behavior of $G(x)$ provided $\widetilde{\zeta} = \exp(-Mv_0)$ is replaced by

$$\zeta(T, h_1, M) = \frac{w\sqrt{AB}(w - w^{-1})^2}{(Aw - 1)(Bw - 1)} e^{-Mv_0}. \qquad (9)$$

The prefactor in Eq. (9) is due to the point tension τ_p (a 2D analog of the line tension) [18] arising at the points where flat portions of the domain wall meet the inclined one. We calculate this prefactor exactly in Appendix D. The point tension τ_p as a function of temperature for different values of the surface field is shown in Fig. 4.

Finally, comparing with Eq. (3) we find

$$\zeta(T, h_1, M) = e^{-2\tau_p} e^{-Mv_0} = \xi_{\parallel}^{-1}/2, \qquad (10)$$

where $\xi_{\parallel}$ is given by Eq. (48). Thus, the result from the coarse-grained model [Eq. (8)] is formally identical to the exact one provided the fugacity $\widetilde{\zeta}$ is identified with the exact fugacity $\zeta(T, h_1, M)$ containing the point tension.

Moreover, if we consider spins at distance m from the channel and compare Eq. (7) with the exact calculation for the full Ising strip, then the prefactor G_0 of the exponential decay can be identified with the amplitude $\bar{\mathrm{m}}_m^2(M)$ in Eq. (47).
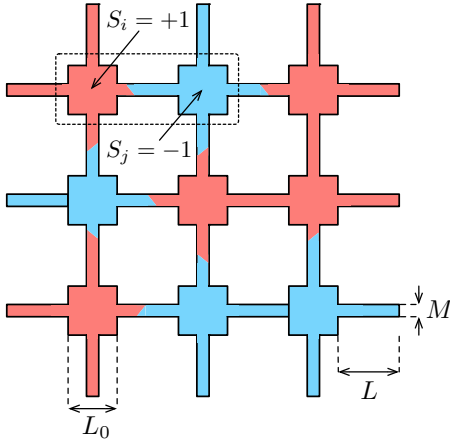
FIG. 5. Geometry of the two-dimensional array of cubes of size L_0 connected by channels (strips) of length L and thickness $M \ll L$. Different colors indicate oppositely magnetized regions. In the "network" Ising model the state of a bulklike box is describe by a spin variable $S_i = \pm 1$.

III. NETWORK PLANAR ISING MODEL

We now apply the mesoscopic description to a pair of cubic lattice boxes of side L_0 coupled by an Ising strip with wetting boundaries of dimension $L \times M$, with $L_0 \gg M$ as shown in Fig. 5. For $T < T_w$, the picture which emerges is one with a sequence of inclined domain walls crossing the strip but none inside the boxes. The domain walls intersecting the boxes are of size $\sim L_0^{d-1}$ and are therefore suppressed due to the much higher cost of free energy. Because boxes are large, we expect that below the wetting temperature $T_w(d = 2)$, which is lower than the critical temperature $T_c(d = 2)$, which in turn is lower than $T_c(d = 3)$, the state of each box is either magnetized up or down. Within our coarse-grained description, we can assign a variable $S_j = \pm 1$ for each box as illustrated in Fig. 5 and calculate a strip-mediated effective interaction energy $K_{\text{eff}} S_i S_j$ for a given argument of the S_j. This can be done by noticing that if spins on neighboring boxes i and j are parallel, that is, $S_i S_j = 1$, then there must be an even number of domain walls on the connecting strip which has length L. On the other hand, if $S_i S_j = -1$, then the location of the spins is separated by an odd number of domain walls. As follows from the previous section, the grand partition function with an even number of particles, denoted $\Xi_e(\ell)$ for a lattice of length $L = \sigma \ell$, is just

$$\Xi_e(\ell) = \sum_{m=0,\text{even}}^{\ell} \binom{\ell}{m} \widehat{\zeta}^m = 2^{-1}\{(1+\widehat{\zeta})^\ell + (1-\widehat{\zeta})^\ell\}. \quad (11)$$

The analogous result for an odd number of particles is

$$\Xi_o(\ell) = \sum_{m=0,\text{odd}}^{\ell} \binom{\ell}{m} \widehat{\zeta}^m = 2^{-1}\{(1+\widehat{\zeta})^\ell - (1-\widehat{\zeta})^\ell\}. \quad (12)$$

Thus the weight of a strip for given spin variables S_i, S_j can be written in an Ising form

$$B(S_i, S_j) = \Xi_e^{(1+S_iS_j)/2} \Xi_o^{(1-S_iS_j)/2} = \mathcal{A}e^{K_{\text{eff}}S_iS_j}, \quad (13)$$

where $\mathcal{A}^2 = \Xi_e(\ell)\Xi_o(\ell)$ and the coupling K_{eff} is given by $e^{2K_{\text{eff}}} = \Xi_e(\ell)/\Xi_o(\ell)$. The equation for the coupling K_{eff} can

be rewritten as:

$$\ell \ln[(1+\widehat{\zeta})/(1-\widehat{\zeta})] = \ln \coth K_{\text{eff}}. \quad (14)$$

We stress here that the temperature evidently does not enter in the usual Boltzmann way in K_{eff}, which has interesting physical consequences, as will be shown in the following.

Having constructed effective bonds, we can now assemble them and boxes to make up a two-dimensional "network" lattice as illustrated in Fig. 5. The long-range order will appear in this network if the parameters can be tuned such that K_{eff} satisfies $K_{\text{eff}} > K_c(d = 2) = (1/2)\ln(1+\sqrt{2}) \approx 0.440687$ [37]. Thus, if the geometrical parameters L, M, and the intensive thermodynamic variables h_1 and T satisfy the following inequality:

$$\ell \ln[(1+\widehat{\zeta})/(1-\widehat{\zeta})] < \ln(1+\sqrt{2}), \quad (15)$$

then the network lattice is ferromagnetically ordered. Given any integer-valued M of the width of the connecting strip, the surface field h_1 and temperature $T < T_w(h_1)$, it is always possible to choose a critical integer-valued ℓ_c for which left- and right-hand sides of Eq. (15) are equal. Because $\widehat{\zeta}$ is small away from the wetting temperature ($w = 1$), we can write

$$\frac{L_c}{\xi_\parallel} = \ln(1+\sqrt{2}), \quad (16)$$

which implies that L_c diverges exponentially with M. The phase diagram of the two-dimensional "network" lattice shown in Fig. 6 for two values of the surface fields corresponding to $T_w = 2.2571$ ($|h_1|/K_2 = 0.1$) and $T_w = 1.40966$ ($|h_1|/K_2 = 0.8$). Notice that for temperatures $T/T_w \lesssim 0.8$, the bulk correlation length does not exceeds $\xi_b \approx 2$, while already at $M = 12$ and $T/T_w = 0.8$ the critical length is $L_c \approx 400$ for $|h_1|/K_2 = 0.1$ and $L_c \approx 4050$ for $|h_1|/K_2 = 0.8$.

Equation (16), which determines the phase boundary between order and disorder phase of array of boxes in a parameter space spanned by temperature and size of connecting strip is the central result of this paper.

IV. STRIPS WITH OPPOSING SURFACE FIELDS: EXACT RESULTS

In this section we determined the length $\xi_\parallel$ from the decay of the correlation function $\mathcal{G}_M(m, n)$ of two spins in the mth row separated by n columns (see Fig. 7). We calculate $\mathcal{G}_M(m, n)$ exactly using the transfer matrix method. In the limit of $L \to \infty$ and for finite M, the leading asymptotic decay of $\mathcal{G}_M(m, n)$ for $n \gg M$ is given by $(\Lambda_2/\Lambda_1)^n = \exp(-n/\xi_\parallel)$ (see, e.g., Ref. [38]), where Λ_1 and Λ_2 are the two largest eigenvalues of the transfer matrix. The analysis of the spectrum of the transfer matrix presented in Sec. IV B shows that below the wetting temperature these two eigenvalues correspond to the imaginary wave numbers $k_1 = iv_1$ and $k_2 = iv_2$, which are asymptotically degenerate. Thus the parallel correlation length is determined by the inverse mass gap between two asymptotically degenerate imaginary modes,

$$\xi_\parallel^{-1} = \gamma(iv_2) - \gamma(iv_1). \quad (17)$$

The Onsager function [37] $\gamma(iv_k), k = 1, 2$ is calculated from $\cosh\gamma(iv_k) = \cosh 2K_1^\star \cosh 2K_2 - \sinh 2K_1^\star \sinh 2K_2 \cosh v_k$, where $\exp(-2K_k^\star) = \tanh K_k$.
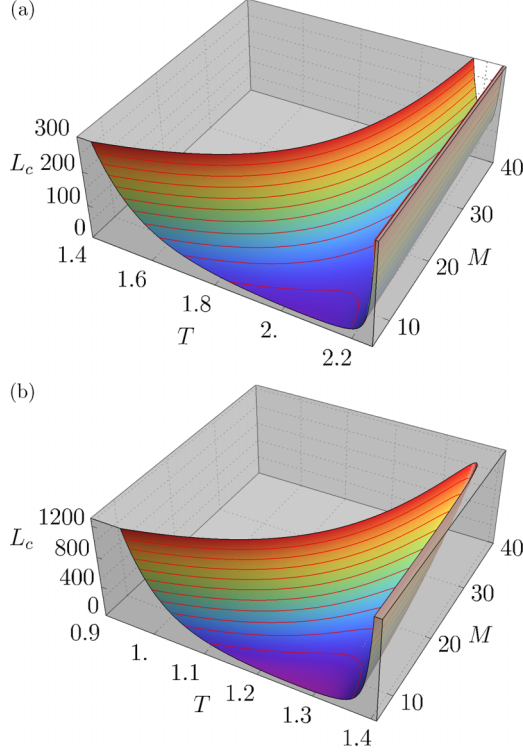
(a)

(b)

FIG. 6. The critical value of the length of connecting strips L_c of the two-dimensional "network" lattice shown in Fig. 5 as a function of the width of the strip M and temperature T for two values of the reduced surface field (a) $h_1/K_2 = 0.1$ corresponding to $T_w = 2.2571$ and (b) $h_1/K_2 = 0.8$ corresponding to $T_w = 1.40966$. The network is ordered in the gray region lying below the critical surface $L_c(M, T, h_1)$.

The microscopic analysis of the two creation operators for the two imaginary wave-number modes (see Sec. IV D for details) enables us to write down states which locate the interface near either one edge or near the other. Thus these states, which are "not quite" eigenvectors of the transfer matrix in the diagonalization, correspond to two phases pseudocoexisting in the partial wetting regime. We now specify the model more precisely.
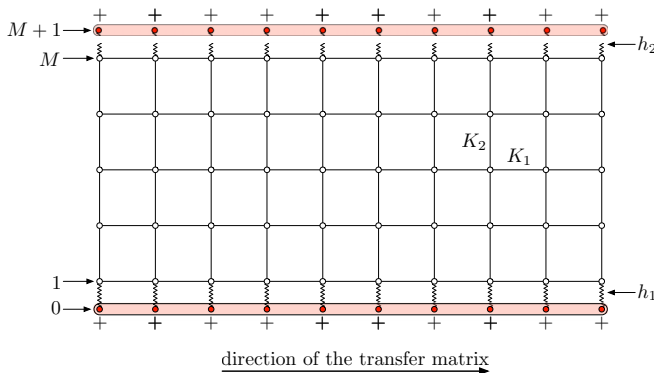

FIG. 7. Ising model on a rectangular lattice (strip) with surface fields h_1 and h_2 as described in the text. The ghost rows with labels $m = 0$ and $m = M + 1$ are indicated in red.

A. Ising model and transfer matrix

We consider a planar Ising ferromagnet in strip geometry with a zero magnetic field. We introduce lines of weakened bonds $|h_1|, |h_2| < K_2$ normal to and contiguous with the surfaces as shown in Fig. 7. We set $\sigma_{n,0} = \sigma_{n,M+1} = +1$ and allow h_1 and h_2 to take both signs. In the following, we only consider the perfectly antisymmetric cases $h_1 = -h_2$. We construct transfer matrix working in (1,0) direction, i.e., parallel to the edges. The column to column (see Fig. 7) transfer operator is given by:

$$\mathsf{V}_1 = (2 \sinh 2K_1)^{M/2} \exp\left[- K_1^\star \sum_{m=1}^{M} \sigma_m^z \right], \qquad (18)$$

where $\tanh K_1 = e^{-2K_1^\star}$. The intrarow couplings along the surface rows $m = 0$ and $m = M + 1$ is $K_0 \to \infty$. The dual coupling $K_0^\star \to 0$, and therefore the indexes $m = 0$ and $m = M + 1$ do not report in (18). Here σ_m^i, $i = x, y, z$ are spin operators[1] with *ordered* direction taken as x, i.e., the magnetization is given by the average of σ_m^x [39]. The transfer matrix V_2 which accounts for the interactions within columns is of the diagonal form

$$\mathsf{V}_2 = \exp\left[h_1 \sigma_0^x \sigma_1^x + K_2 \sum_{m=1}^{M-1} \sigma_m^x \sigma_{m+1}^x + h_2 \sigma_M^x \sigma_{M+1}^x \right]. \qquad (21)$$

As noted by Kaufman [40], in order to diagonalize the symmetrized forms of the transfer operators it is essential to introduce the Jordan-Wigner transformation and the lattice spinors Γ_m defined by

$$\Gamma_{2m-1} = \mathcal{P}_{m-1} \sigma_m^x,$$
$$\Gamma_{2m} = \mathcal{P}_{m-1} \sigma_m^y, \quad \text{for } m = 1, \dots, M + 1, \qquad (22)$$

supplemented with $\Gamma_{-1} = \sigma_0^x$ and $\Gamma_0 = \sigma_0^y$, and where

$$\mathcal{P}_m = \prod_{j=0}^{m} (-\sigma_j^z), \qquad (23)$$

is the "fermionic tail." The spinors we just introduced are self-adjoint operators with square equal to unity, and they anticommute with each other and fulfill the Clifford algebra,

$$[\Gamma_m, \Gamma_n]_+ = 2\delta_{m,n}. \qquad (24)$$

The spinors are related to the fermionic operators $X(k)$, $k = 1, \dots, M$ by

$$X(k) = \frac{1}{2} N(k) \sum_{m=0}^{2M+1} y_m(k) \Gamma_m, \qquad (25)$$

---

[1]The operator σ_m^α acts on the tensor product of the two-dimensional Hilbert spaces of each lattice site in a column

$$\sigma_m^\alpha = \bigotimes_{j=1}^{m-1} \mathbf{1} \bigotimes \sigma^\alpha \bigotimes_{j=m+1}^{M} \mathbf{1}, \qquad (19)$$

where σ^α, $\alpha = x, y, z$ are Pauli matrices. In particular σ_m^α fulfills the on-site anticommutation relation

$$[\sigma_m^\alpha, \sigma_m^\beta]_+ = 2\delta_{\alpha\beta}, \qquad (20)$$

while for $n \neq m$, $[\sigma_m^\alpha, \sigma_n^\beta]_- = 0$.

where the normalization factor $N(k)$ ensures the canonical anticommutation relation, i.e., $[X(k_1), X^\dagger(k_2)]_+ = \delta_{k_1,k_2}$. The functions $y_m(k)$ have to be determined such that in terms of $X(k)$ and $X^\dagger(k)$ the transfer operator $\mathsf{V} = \mathsf{V}_2^{1/2} \mathsf{V}_1 \mathsf{V}_2^{1/2}$ admits the diagonal form

$$\mathsf{V} = \exp\left[- \sum_{k \in \Omega_M} \gamma(k)\big(X^\dagger(k)X(k) - 1/2\big) \right], \qquad (26)$$

where $\gamma(k)$ is the non-negative solution of

$$\cosh \gamma(k) = \cosh 2K_1^\star \cosh 2K_2 - \sinh 2K_1^\star \sinh 2K_2 \cos k, \qquad (27)$$

for real k. Note that operators associated with Γ_{-1} and $\Gamma_{2(M+1)}$, $X_0 = (1/2)[\Gamma_{-1} + i\Gamma_{2(M+1)}]$ and its conjugate, do not appear in (26). They are zero-energy operators, which implies that each eigenvalue is doubly degenerate. We denote the vacuum[2] for the operators $X(k)$ and X_0, which is also the maximal eigenvector with eigenvalue Λ_0, by $|\Phi_\infty\rangle$. The vacuum $|\Phi_\infty\rangle$ includes all four possible cases in which the spins in a given edge are parallel. The spectrum for the edge state corresponding to $h_1 < 0$ and $h_2 > 0$ is constructed with the use of appropriate projectors [14,35]

$$X^\dagger((k)_{2n+1})|++\rangle, \qquad (28)$$

where the notation in the above is

$$X^\dagger((k)_n) = X^\dagger(k_1) \cdots X^\dagger(k_n), \qquad (29)$$

and

$$|++\rangle = 2^{-1/2}(1 + X_0^\dagger)|\Phi_\infty\rangle, \qquad (30)$$

is the normalized state with plus boundary spins. For the case of $h_1 > 0$ and $h_2 < 0$, the spectrum is constructed by replacing $|++\rangle$ in Eq. (30) by the state $|--\rangle = 2^{-1/2}(1 - X_0^\dagger)|\Phi_\infty\rangle$. The sum appearing in (26) is restricted to wave numbers k compatible with the boundary conditions on the edges of the strip. This generates the following discretization condition [14]:

$$e^{iMk} = se^{i\delta(k)} = se^{i\delta'(k)} \frac{we^{ik} - 1}{e^{ik} - w}, \qquad (31)$$

whose solutions define the set Ω_M. The parity number $s = \pm 1$ encodes reflection behavior of the eigenvectors, $\delta'(k)$ is the angle introduced by Onsager (see Appendix C), and w is the wetting parameter [Eq. (1)]. For the V symmetrization we have

$$y_{2m+1}(k) = -e^{-i\delta^*}e^{imk} + e^{i\delta}e^{-imk},$$
$$y_{2m}(k) = i(-e^{imk} + e^{i\delta}e^{-i\delta^*}e^{-imk}),$$
$$m = 1, \ldots, M-1, \qquad (32)$$

with the boundary values

$$y_0(k) = i\sqrt{\frac{B}{B-w}}(-1 + e^{i\delta}e^{-i\delta^*})$$
$$\qquad (33)$$
$$y_1(k) = \sqrt{\frac{A}{A-w}}(-e^{-i\delta^*} + e^{i\delta}),$$

---

[2]The vacuum $|\Phi_\infty\rangle = X_0|\Phi\rangle$, where $|\Phi\rangle$ is a vacuum determined by $X(k)|\Phi\rangle = 0$ for all $k \in \Omega_M$.

where $A = \exp[2(K_1 + K_2^\star)]$ and $B = \exp[2(K_1 - K_2^\star)]$. The quantities $y_{2M}(k)$ and $y_{2M+1}(k)$ are obtained by using the reflection symmetry:

$$y_{2(M+1-m)} = -is\, y_{2m-1},$$
$$y_{2(M-m)+1} = is\, y_{2m}. \qquad (34)$$

B. Asymptotic degeneracy

In order to proceed it is crucial to discuss the allowed momenta k for subcritical temperatures $K_2 > K_1^\star$. We restrict k to the range $[0, \pi]$. At $T_w(h_1)$ there is a special solution at $k = 0$ with nonzero eigenvector and the corresponding eigenvalue $\Lambda_0 \exp[\gamma(0)]$. For all other temperatures the values $k = 0$ and $k = \pi$ give trivial eigenvectors. In the partially wet regime $T < T_w(h_1)$ there are $M - 2$ real solutions between 0 and π. Two solution of the discretization condition (31) are found at imaginary values $k_1 = iv_1$ and $k_2 = iv_2$ [14]:

$$v_1 \simeq v_0 - \mathcal{A}(T, h_1)w^{-M}, \quad (s = +1)$$
$$v_2 \simeq v_0 + \mathcal{A}(T, h_1)w^{-M}, \quad (s = -1), \qquad (35)$$

with $v_0 = \ln w$ and

$$\mathcal{A}(T, h_1) = \left(\frac{A-w}{Aw-1} \frac{B-w}{Bw-1} \right)^{1/2} (w - w^{-1}). \qquad (36)$$

The symbol $\simeq$ in Eq. (35) denotes the omission of subdominant terms of order w^{-2M}. Note that below bulk criticality ($B > 1$) and within the wetting regime ($w > 1$) each factor in (36) is strictly positive since $A > B > w > 1$. The imaginary modes give rise to two asymptotically degenerate eigenvectors given by

$$X^\dagger(iv_1)|++\rangle \quad \text{and} \quad X^\dagger(iv_2)|++\rangle, \qquad (37)$$

with eigenvalues

$$\Lambda_1 = \Lambda_0 e^{-\gamma(iv_1)} \quad \text{and} \quad \Lambda_2 = \Lambda_0 e^{-\gamma(iv_2)}. \qquad (38)$$

Because $\gamma(iv_1) < \gamma(iv_2) < \gamma(0)$, whereas $\gamma(k)$ corresponding to the real k are all larger then $\gamma(0)$, these two asymptotically degenerate eigenvectors are the lowest excitation states. The asymptotic degeneracy of the transfer matrix spectrum disappears at temperature $\sim T_w(h_1) - C(h_1)/M$. For $T > T_w(h_1)$ all momenta k are real.

C. Diverging length scale

Let us consider the pair-correlation function $\mathcal{G}_M(m, n) = \langle \sigma_{m,l} \sigma_{m,l+n} \rangle - \langle \sigma_{m,l} \rangle \langle \sigma_{m,l+n} \rangle$ of two spins in the mth row separated by n columns (see Fig. 7). Using the transfer matrix we can write

$$\mathcal{C}_M(m, n) = \langle \sigma_{m,l} \sigma_{m,l+n} \rangle = \frac{\text{Tr}\big(\mathsf{V}^{L-n}\sigma_m^x \mathsf{V}^n \sigma_m^x\big)}{\text{Tr}(\mathsf{V}^L)}, \qquad (39)$$

where we have imposed periodic boundary conditions in the strip axial direction. For the edge state corresponding to $h_1 < 0$ and $h_2 = -h_1$, Eq. (39) reduces in the limit of $L \to \infty$ to

$$\mathcal{C}_M(m, n)$$
$$= \langle ++ |X(iv_1)\sigma_m^x(\mathsf{V}/\Lambda_{\max})^n \sigma_m^x X^\dagger(iv_1)|++\rangle, \qquad (40)$$

where $\Lambda_{\max} = \Lambda_0 \exp[-\gamma(iv_1)]$. By applying the spectral decomposition to V we find that the lowest-order contributions to $\mathcal{C}_M(n)$ come from the one-particle states, i.e., from

$$\sum_{k \in \Omega_M} \Lambda_k^n X^\dagger(k) \big(|\Phi_\infty\rangle\langle\Phi_\infty| + X_0^\dagger|\Phi_\infty\rangle\langle\Phi_\infty|X_0 \big) X(k), \quad (41)$$

where $\Lambda_k = \Lambda_0 \exp[-\gamma(k)]$ is the eigenvalue of $X^\dagger(k)|\Phi_\infty\rangle$ as well as of $X^\dagger(k)X_0^\dagger|\Phi_\infty\rangle$. Therefore we have

$$\mathcal{C}_M(m,n) \simeq \sum_{k \in \Omega_M} |\langle + + |X(iv_1)\sigma_m^x X^\dagger(k)| + +\rangle|^2$$
$$\times e^{-n(\gamma(k)-\gamma(iv_1))}. \quad (42)$$

The spectral sum can be split into a sum over the states with imaginary wave numbers and a remainder stemming from the real wave numbers. This generates three different types of contributions. The wave number $k_1 = iv_1$ gives a n-independent contribution

$$\mathfrak{m}_m^2(M) = |\langle + + |X(iv_1)\sigma_m^x X^\dagger(iv_1)| + +\rangle|^2, \quad (43)$$

which is the formula for the square of magnetization $\mathfrak{m}_m(M) = \langle\sigma(m,l)\rangle$ at the row m of the strip [14]. From the wave number $k_2 = iv_2$ we have a n-dependent contribution,

$$|\langle + + |X(iv_1)\sigma_m^x X^\dagger(iv_2)| + +\rangle|^2 e^{-n[\gamma(iv_2)-\gamma(iv_1)]}, \quad (44)$$

whereas the real wave numbers generate terms which are proportional to

$$\exp\{-n[\gamma(k) - \gamma(iv_1)]\}. \quad (45)$$

By virtue of the inequality $\gamma(k) > \gamma(iv_2) > \gamma(iv_1)$, provided k is real the terms of the form (45) decay on a shorter length scale compared to (44), and therefore they yield subleading corrections beyond the leading decay given by Eq. (44). Because in the partial wetting regime (below the wetting temperature)

$$\min_{k \in \Omega_M} [\gamma(k) - \gamma(iv_1)] > \gamma(iv_2) - \gamma(iv_1), \quad (46)$$

for $n \to \infty$ we can write

$$\mathcal{G}_M(m,n) = \mathcal{C}_M(m,n) - \mathfrak{m}_m^2(M) \simeq \bar{\mathfrak{m}}_m^2(M)e^{-n/\xi_\parallel}, \quad (47)$$

where $\simeq$ stands for the omission of subleading terms due to real wave numbers and $\bar{\mathfrak{m}}_m(M) = |\langle + + |X(iv_1)\sigma_m^x X^\dagger(iv_2)| + +\rangle|$. Although the factor $\bar{\mathfrak{m}}_m(M)$ depends on the distance from the edges, the decay of the correlation function is always exponential. Then, for largely separated spins, the connected correlation function tends to zero, as it should. As follows from Eqs. (27) and (35) [see also Eq. (D9)], the length scale $\xi_\parallel$, on which long-range order is ultimately lost, diverges exponentially fast as $M \to \infty$ [14],

$$\xi_\parallel = \frac{(Aw-1)(Bw-1)}{2w\sqrt{AB}(w-w^{-1})^2}w^M, \quad (48)$$

with $w = e^{v_0}$. In Appendix E we calculate the edge magnetizations $\mathfrak{m}_1(M)$ and $\bar{\mathfrak{m}}_1(M)$ entering the expression of the spin-spin correlation function for spins placed on the edge. We find $\mathfrak{m}_1(M) = -\mathfrak{m}_e + O(w^{-M}) + O(M^{-3/2}e^{-2M\hat{\gamma}(0)})$, where $\mathfrak{m}_e$ is the surface magnetization in the semiinfinite system with
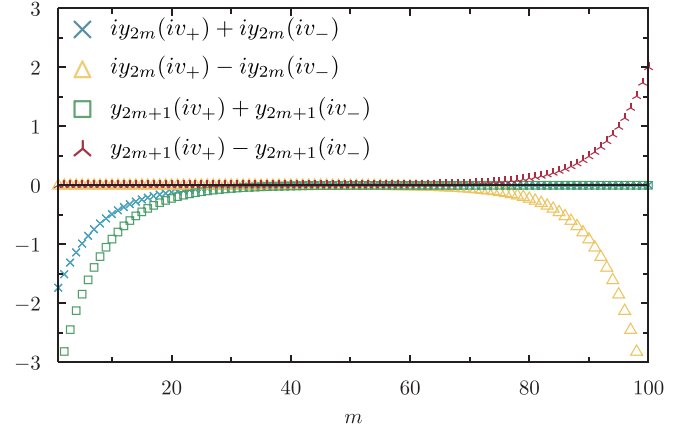

FIG. 8. Even and odd combinations of eigenvectors of the transfer matrix V. In this figure, $K_1 = K_2$, the temperature is $T = 2$ and the surface field is $h_1 = 0.3$, corresponding to $w = 1.1513$.

a positive surface field (result for $\mathfrak{m}_e$ was also obtained using the Pfaffian method [41,42]):

$$\mathfrak{m}_e \simeq \frac{w - w^{-1}}{\sqrt{(w - A^{-1})(w - B^{-1})}}$$
$$+ \left[\frac{AB}{(A-w)(B-w)}\right]^{1/2} \int_{-\pi}^{\pi} \frac{dk}{2\pi} [\cos\delta^*(k) - \cos\delta(k)], \quad (49)$$

and

$$\bar{\mathfrak{m}}_1(M) = \frac{w - w^{-1}}{\sqrt{(w - A^{-1})(w - B^{-1})}} + O(w^{-M}). \quad (50)$$

D. Surface states

We note that the sums and differences of eigenvectors $\mathcal{E}_m^\pm = iy_{2m}(iv_1) \pm iy_{2m}(iv_2)$ and $\mathcal{O}_m^\pm = y_{2m+1}(iv_1) \pm y_{2m+1}(iv_2)$, respectively with $+$ and $-$, decay exponentially from one or the other edge of the strip. In particular, the sums $\mathcal{E}_m^+$ and $\mathcal{O}_m^+$ decay exponentially from the bottom edge at $m = 0$, whereas the differences exhibit an exponential decay from the top boundary $m = M + 1$; see Fig. 8. This can be seen as follows. By using the discretization equation, (32) becomes

$$y_{2m+1}(iv) = -e^{i\delta^*(iv)}e^{-mv} + se^{-(M-m)v}. \quad (51)$$

The above clearly displays a linear combination of exponentially evanescent terms fading out from the two edges. By using (51), the combination $\mathcal{O}_m^+$ becomes

$$\mathcal{O}_m^+ = y_{2m+1}(iv_1) + y_{2m+1}(iv_2)$$
$$= [-e^{-i\delta^*(iv_1)-mv_1} - e^{-i\delta^*(iv_2)-mv_2}]$$
$$+ [e^{-(M-m)v_1} - e^{-(M-m)v_2}]. \quad (52)$$

Since v_1 and v_2 are exponentially degenerate for large M, the two terms in the first bracket become equal for large M, while the terms in the second square bracket almost cancel each other, leaving an exponentially subleading correction. Therefore we obtain $\mathcal{O}_m^+ \simeq -2\exp[-i\delta^*(iv_0)]\exp(-mv_0)$, which corresponds to an interface running bound to the edge $m = 0$;
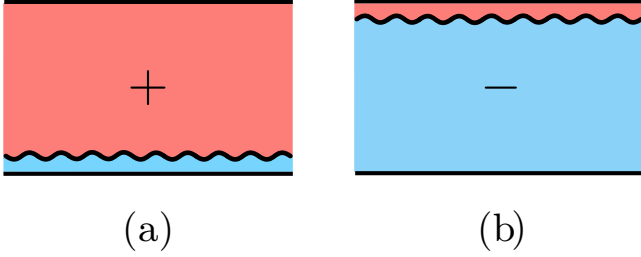
FIG. 9. Depiction of a domain wall bound to the wall at $m = 0$ (a) and at $m = M + 1$ (b).

see the green squares in Fig. 8. A similar analysis can be carried out for the remaining combinations.

This behavior suggests the construction of the following even-odd combination for putative surface states:

$$|e\rangle = 2^{-1}[X^\dagger(iv_1) + X^\dagger(iv_2)](1 + X_0^\dagger)|\Phi_\infty\rangle,$$

$$|o\rangle = 2^{-1}[X^\dagger(iv_1) - X^\dagger(iv_2)](1 + X_0^\dagger)|\Phi_\infty\rangle. \quad (53)$$

Note that these states are not the eigenstates of the transfer matrix. It can be shown that as $M \to \infty$ they have the property

$$\langle o|\sigma_1^x|o\rangle = -\mathfrak{m}_e \quad \text{and} \quad \langle e|\sigma_M^x|e\rangle = \mathfrak{m}_e. \quad (54)$$

We refer to Appendix E for details of the calculations of the edge magnetizations. We can see that if $n = x/a$, where $a = 1$ is the lattice constant, then

$$\mathsf{V}^n|e\rangle = 2^{-1}\Lambda_0 e^{-\gamma(iv_1)}[X^\dagger(iv_1) + e^{-n/\xi_\parallel}X^\dagger(iv_2)](1 + X_0^\dagger)|\Phi_\infty\rangle. \quad (55)$$

Therefore, the system initially prepared in the state $|e\rangle$ loses coherence over a length scale $\xi_\parallel$. This feature is characteristic of the tunneling phenomenon between the two states in which the interface runs close to one or the other edge. Thus, $|e\rangle$ and $|o\rangle$ can be interpreted as states in which the domain wall is bound to the one side of the strip or to the other one, as sketched in Fig. 9. It is straightforward to show that

$$\Lambda_1^{-n}\langle e|\mathsf{V}^n|e\rangle = 2^{-1}[1 + \exp(-n/\xi_\parallel)],$$

$$\Lambda_1^{-n}\langle o|\mathsf{V}^n|e\rangle = 2^{-1}[1 - \exp(-n/\xi_\parallel)]. \quad (56)$$

If $n \gg \xi_\parallel$, then the elements of transition matrix tend to $1/2$. This means that the system flips between different surface states on the length scale $\xi_\parallel$. Finally, we notice an interesting analogy between the ratio of the above matrix elements and the ratio of grand partition functions Ξ_o/Ξ_e with an odd and even number of particles in the mesoscopic description of the Ising strip discussed in Sec. II. We have

$$\frac{\langle o|\mathsf{V}^n|e\rangle}{\langle e|\mathsf{V}^n|e\rangle} = \tanh \frac{n}{2\xi_\parallel} \quad (57)$$

and in the dilute limit $\widehat{\zeta} = \sigma\widetilde{\zeta} \ll 1$

$$\frac{\Xi_o(x)}{\Xi_e(x)} \simeq \tanh \frac{n}{\underset{\approx}{\zeta}}, \quad (58)$$

where $x = \sigma n$. Because of the exact identity $\zeta = (2\xi_\parallel)^{-1}$, Eqs. (57) and (58) are formally equivalent provided the fugacity $\widetilde{\zeta} = \exp(-Mv_0)$ used in the mesoscopic picture (see

Sec. II) is identified with the exact one [Eq. (10)] containing the point tension.

V. SUMMARY AND CONCLUSIONS

In this paper we have studied a network Ising model constructed from a 2D array of boxes and connecting strips with wetting boundaries. We have showed that in the partial wetting regime, the parameters can be tuned to produce long-range order. If the connecting channels are long enough, then the ordering between boxes extends over many thousands of molecular diameters. We expect the similar scenario for surface fields that are marginally long ranged [43]. The above phenomenon is in sharp contrast with the exponential decay of order in a bulk system in which the decay takes place on the scale of the bulk correlation length. It has been shown rather recently that a classical system supports such a type of order with free boundary conditions [5] and that this effect is not a prerogative of inherently quantum systems. However, the potential feasibility of free boundaries in experiments with binary liquid mixtures at the walls requires fine tuning of the interactions between the walls and the fluid components, because in general the walls tend to be wetted by one component more than the other. This experimental fact motivated the present study of surface fields acting on the boundaries. One of the most important results we obtained is that the above mentioned long-range ordering known for free boundaries protracts also for surface fields. Our theory, which applies to classical lattice gases and their analogs, maybe tested in Monte Carlo simulations [44] and in experiments. In the context of the latter, it should be noted that the long-range order in our system is based on the asymmetry of the connecting channels, which may be difficult to achieve in the case of fluids. We expect that the use of a bulk ordering field h could compensate for the slight violation of the asymmetry of the surface fields. However, this possibility is limited to the extremely small range of h centered around $h = 0$ because, as predicted by the Fisher-Privman theory of finite-size scaling in first-order phase transitions [16], the correlation length $\xi_\parallel$ in the strip is only exponentially in M large provided the bulk magnetic field h is exponentially small in M. Other realistic physical conditions that may influence the long-range order in the network are, for example, the roughness of the channels or the fact that their widths are not the same but subject to a random distribution. Investigating this latter effect would require considering a network Ising lattice model with random bonds. Regarding the roughness effect, it is very likely that pinning the domain wall to rough surfaces would prevent it from switching from one side of the strip to the other and thus destroy asymptotic degeneracy and thus long-range order.

Our paper also contains, to the best of knowledge, new exact results regarding the Ising model in two dimensions. We have given a microscopic analysis of surface states for the Ising strip with opposing surface fields. Surface states produce an asymptotic degeneracy of the transfer matrix in a partial wetting region [10]. We calculated exactly the free energy associated with a domain wall running at the angle to the edges of the strip and the point tension for boundaries subject to surface fields.
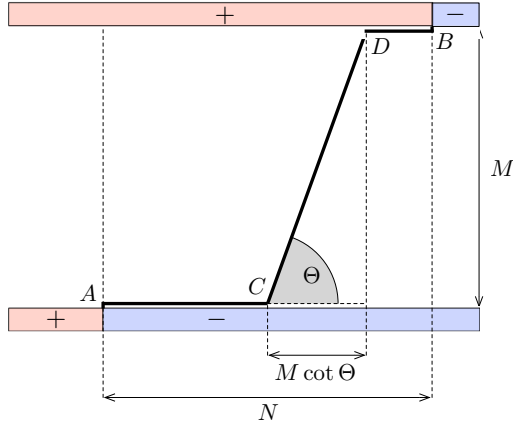
FIG. 10. A domain wall composed of two flat pieces running parallel to the wall and section inclined at an angle Θ (called wetting angle). The optimal value of $M \cot \Theta$ is obtained by minimizing the excess free energy associated with such an interfacial configuration.

ACKNOWLEDGMENTS

APPENDIX A: CONTACT ANGLE

Consider a strip with boundary conditions that introduce a domain wall pinned on two edges, as shown in Fig. 10. The pinning points are offset by N in the horizontal direction and M in the vertical direction. In the presence of surface fields at the boundaries, the surface attracts the domain wall, and, therefore, below the wetting temperature, the domain wall cannot be a straight line connecting the pinning points at the edges of the strip. Rather, it will adopt the shape shown in Fig. 10 with the contact angle that can be determined from minimization of the excess free energy associated with such a domain wall. Let f_0 be the surface free energy of a flat interface pinned to the wall and let $\tau(\vartheta)$ be the angle-dependent surface tension [35,36] for an inclined interface forming a tilt angle ϑ with the wall as shown in Fig. 10. The angle-dependent surface tension was calculated in the case where there is no attracting bonds at the edges, i.e., for $|h_1| = |h_2| = K_2$, in Ref. [35]; it satisfies

$$\tau(\vartheta) = (\cos \vartheta)\gamma[iv_s(\vartheta)] + (\sin \vartheta)v_s(\vartheta), \quad (A1)$$

with $v_s(\vartheta)$ given by the saddle-point calculations as [36]

$$\gamma^{(1)}[iv_s(\vartheta)] = i \tan \vartheta, \quad (A2)$$

where here the superscript denotes the first derivative with respect to k of Onsager's $\gamma(k)$ function given by Eq. (27). Thus the excess free energy for the domain wall shown in

Fig. 10 can be written as

$$\mathcal{F}(\vartheta) = (M \csc \vartheta)\tau(\vartheta) + (N - M \cot \vartheta)f_0 - Nf_0. \quad (A3)$$

The first term is due to the inclined interface, and the second is due to the horizontal portions. The third term is the free energy for a flat interface pinned to the wall; the subtraction ensures that $\mathcal{F}(\vartheta)$ is actually the *excess* free energy. Now we look for the wetting angle Θ which minimizes the function $\mathcal{F}(\vartheta)$. By using the identity

$$\tau'(\vartheta) = -(\sin \vartheta)\gamma[iv_s(\vartheta)] + (\cos \vartheta)v_s(\vartheta), \quad (A4)$$

which follows from (A1) and (A2), we find

$$\partial_\vartheta \mathcal{F}(\vartheta) = M \csc^2 \vartheta\{f_0 - \gamma[iv_s(\vartheta)]\}. \quad (A5)$$

The stationary condition gives

$$f_0 = \gamma[iv_s(\Theta)], \quad (A6)$$

in agreement with the result of earlier studies with $v_s = v_0$ [14,25]. This, together with Eq. (A1), leads to a rather compact expression for the excess free energy associated to the insertion of an inclined domain wall,

$$\mathcal{F}(\Theta) = Mv_0(\Theta). \quad (A7)$$

Equation (A2) gives the contact angle Θ as the solution of

$$\frac{s_1^\star s_2 \sinh v_0(\Theta)}{\sinh \gamma[iv_0(\Theta)]} = \tan \Theta, \quad (A8)$$

with the shorthand notation $s_1 = \sinh 2K_1$ and $s_2^\star = \sinh 2K_2^\star$. Hence, if $v_0 \searrow 0$ at the wetting transition, then $\Theta \searrow 0$ as anticipated. In Appendix D we will demonstrate by exact microscopic calculation of $\mathcal{F}(\Theta)$ that indeed $v_s(\Theta)$ in Eq. (A6) is equal to $v_0 = \ln w$. Figure 11 shows the contact angle Θ as a function of the surface field and temperature.

APPENDIX B: HARD ROD LATTICE GAS AND THE TONKS GAS

Proceeding with the exact grand partition function of the hard rod lattice gas given by Eq. (4) is not a simple task. For this reason it makes sense to find a way to simplify the expression of the partition function. At this point it is very useful to show how we can approximate the hard rod lattice gas with a Tonks-Rayleigh hard rod gas in the continuum [32,33]. Recall that the canonical partition function of Tonks-Rayleigh hard rod gas with j particles on the line of length L in the absence of any external potential is equal to

$$\mathcal{Q}_j^{\text{Tonks}} = \frac{(L - j\sigma + j)^j}{j!}; \quad (B1)$$

this equation appeared in the seminal paper by Lee and Yang on the theory of equations of state (see Eq. (51) of Ref. [45]).

By applying Stirling's formula to the binomial $\binom{L-j\sigma+j}{j}$ for fixed j and large $L - j\sigma + j$, we find

$$\mathcal{Q}_j^{\text{lattice HR}} = \binom{L - j\sigma + j}{j}$$

$$\approx \frac{(L - j\sigma + j)^j}{j!} = \mathcal{Q}_j^{\text{Tonks}}(L, \sigma - 1), \quad (B2)$$
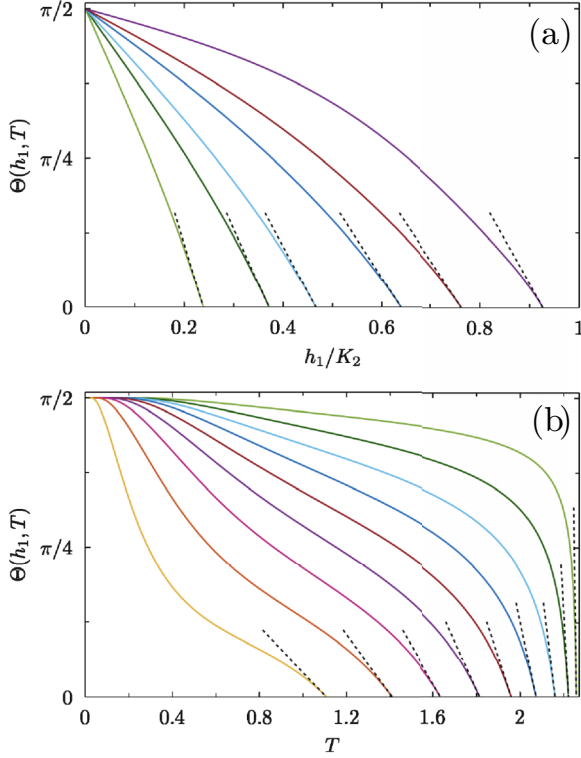
FIG. 11. The contact angle $\Theta(h_1, T)$ as a function of the rescaled field h_1/K_2 for fixed temperature (a), and as a function of the temperature for fixed rescaled field $h_1/K_2 = a$ (b). In panel (a) the temperature takes the values $T = 2.2, 2.1, 2.0, 1.75, 1.5, 1.0$ (from left to right curves). In panel (b) the rescaled field ranges from 0.1 to 0.9 with spacing 0.1 (from top to bottom curves). The dashed black lines in (a) and (b) show the linear vanishing of the contact angle on approaching the wetting phase boundary. In these figures, $K_1 = K_2$.

where $\mathcal{Q}_j^{\text{lattice HR}}$ is the canonical partition function of the lattice hard rods model. Having established a connection between the canonical partition function for hard rods on the lattice and hards rods in the continuum (Tonks gas), we now show how this enables us to simplify the grand partition function [Eq. (4)]. To this end we write the grand partition function of the Tonks gas,

$$\Xi^{\text{Tonks}}(\widetilde{\zeta}, L, \sigma) = \sum_{j=0}^{[L/\sigma]} \widetilde{\zeta}^j (L - j\sigma)^j / j!$$

$$\approx \sum_{j=0}^{[L/\sigma]} (\widetilde{\zeta}\sigma)^j (L/\sigma)^j / j! \approx \sum_{j=0}^{[L/\sigma]} (\widetilde{\zeta}\sigma)^j \binom{L\sigma}{j}$$

$$= (1 + \widetilde{\zeta}\sigma)^{L/\sigma} = \Xi^{\text{lattice gas}}(\widetilde{\zeta}\sigma, L/\sigma),$$

where $\Xi^{\text{lattice gas}}(\zeta, L) = (1 + \zeta)^L$ is the grand partition function for the hard rod gas with unit diameter encountered in the free edge problem. The approximation then connects the Tonks gas to the lattice gas, thus providing a bridge between the continuum and the discrete descriptions of the one-dimensional gases of impenetrable particles. The chain of approximations is valid in the regime of small $\widetilde{\zeta}$, which predominantly weights those configurations with small j. Therefore at small fugacity the Tonks gas behaves as an ideal

lattice gas with enhanced fugacity $\widetilde{\zeta}\sigma$ in a reduced volume L/σ.

APPENDIX C: ONSAGER ANGLES

The functions $\delta'(k)$ and $\delta^*(k)$, introduced by Onsager [37], are elements of a hyperbolic triangle whose edges have length $K_1^\star$, K_2, and $\gamma(k)$. The angle $\delta^*(k)$ is related to the other geometrical elements via

$$c_1^\star = c_2 \cosh \gamma(k) - s_2 \sinh \gamma(k) \cos \delta^*(k), \qquad (C1)$$

which is formally analogous to Eq. (27) [46]. Here we use the following shorthand notation: $s_1^\star = \sinh 2K_1^\star$, $c_1^\star = \cosh 2K_1^\star$, $s_2 = \sinh 2K_2$, and $c_2 = \cosh 2K_2$. Furthermore, by combining the above with Eq. (27) we find

$$\cos \delta^*(k) = \frac{c_1^\star s_2 - s_1^\star c_2 \cos k}{\sinh \gamma(k)}. \qquad (C2)$$

The above angles admit the factorized expressions

$$e^{2i\delta'(k)} = \frac{e^{ik} - A}{Ae^{ik} - 1} \frac{e^{ik} - B}{Be^{ik} - 1}, \qquad (C3)$$

and

$$e^{2i\delta^*(k)} = \frac{e^{ik} - A}{Ae^{ik} - 1} \frac{Be^{ik} - 1}{e^{ik} - B}, \qquad (C4)$$

Physical arguments demand that $\gamma(0) > 0$ for both $T < T_c$ and $T > T_c$. On the other hand, the behavior at $k = 0$ of the Onsager angles depends on the temperature, as can be realized by plugging $k = 0$ into Eq. (C2). For subcritical temperatures ($A > B > 1$) the sheet of the square root is selected such that $\delta^*(0) = 0$, thus $e^{i\delta^*(0)} = +1$. For supercritical temperatures ($B < 1$) we have $\delta^*(0) = \pi$, and hence $e^{i\delta^*(0)} = -1$. An analogous treatment applies to the angle $\delta'(k)$ by noting that it can be obtained by mapping B to B^{-1} in the expression of $\delta^*(k)$. Therefore, for subcritical temperatures $e^{i\delta'(0)} = -1$.

APPENDIX D: BOLTZMANN WEIGHT FOR OPPOSING SURFACE FIELDS

The free energy $F(N, M)$ of the domain wall shown in Fig. 10 can be calculated from a canonical partition function ratio $Z^\times/Z$ for a system with and without a domain wall (see Fig. 12 for clarification of notations) using a transfer matrix approach,

$$Z^\times/Z = \frac{\text{Tr}\left[(\mathsf{V}')^{L-N}(-\sigma_0^z)(\mathsf{V}')^N(-\sigma_{M+1}^z)\right]}{\text{Tr}[(\mathsf{V}')^L]}, \qquad (D1)$$

where L denotes the length of the lattice shown in Fig. 12. [For correlation functions of the Ising system in the geometry of Fig. 12(a) with $N = 0$ and Fig. 12(b) see Refs. [47,48] and Refs. [49,50], respectively.] Technically, the lattice is wrapped onto a cylinder; more correctly, there is another domain wall but it is assumed to be far away. We have used $\mathsf{V}' = \mathsf{V}_1^{1/2}\mathsf{V}_2\mathsf{V}_1^{1/2}$ as symmetrization [40]. This symmetrization is more convenient here because the rotation operators $-\sigma_0^z$ and $-\sigma_{M+1}^z$ involved in (D1) anticommute with V_1. These operators reverse the spins on the bottom $m = 0$ and top $m = M + 1$ edges and thus introduce a domain wall across the strip. For
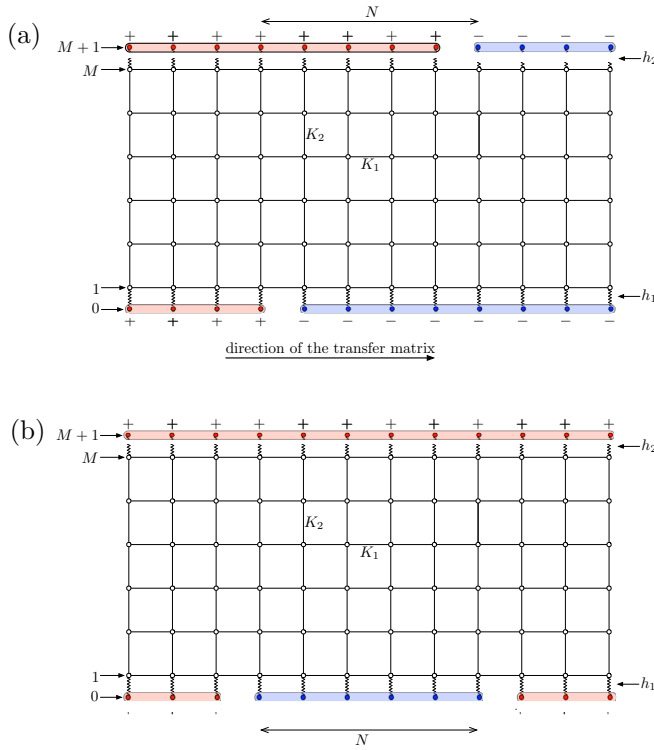
FIG. 12. Lattice used for the calculation of the free energy for the inclined (upper panel) and "flat" (bottom panel) domain walls.

the edge state corresponding to $h_1 > 0$ and $h_2 = h_1$, Eq. (D1) reduces in the limit $L \to \infty$ to

$$e^{-F(N,M)} = \frac{\langle + + |(-\sigma_0^z)(V')^N(-\sigma_{M+1}^z)| - - \rangle}{\langle + + |(V')^N| + + \rangle}, \quad \text{(D2)}$$

where the in- and out-asymptotic states $| + + \rangle$ and $| - - \rangle$ are defined in the same way as in Sec. IV A, but with X_0 in Eq. (30) replaced by X_0' for the V' symmetrization. By using the relations $-\sigma_0^z = i\sigma_0^x\sigma_0^y = i\Gamma_{-1}\Gamma_0 = [X_0' + (X_0')^\dagger]i\Gamma_0$ and $-\sigma_{M+1}^z = i\sigma_{M+1}^x\sigma_{M+1}^y = i\Gamma_{2M+1}\Gamma_{2M+2} = \Gamma_{2M+1}[X_0' - (X_0')^\dagger]$ (see Sec. IV A) and applying the spectral decomposition to the operator V', we find that the lowest-order contributions to $e^{-F(N,M)}$ come from the one-particle states, and therefore

$$e^{-F(N,M)}$$
$$= \sum_{k \in \Omega_M} e^{-N\gamma(k)} \langle \Phi_\infty | i\Gamma_0(X_k')^\dagger | \Phi_\infty \rangle \langle \Phi_\infty | X_k' \Gamma_{2M+1} | \Phi_\infty \rangle.$$
$$\text{(D3)}$$

By using the expressions for Γ_0 and Γ_{2M+1} in terms of Fermi operators [see Eq. (E5)], we find

$$e^{-F(N,M)} = \sum_{k \in \Omega_M} [N'(k)]^2 i[y_0'(k)]^* y_{2M+1}'(k) e^{-N\gamma(k)}, \quad \text{(D4)}$$

where the eigenvectors for the V' symmetrization are as follows:

$$y_{2m-1}'(k) = e^{i\delta'(k)}e^{imk} + e^{i\delta(k)}e^{-i(m-1)k},$$
$$iy_{2m}'(k) = e^{imk} + e^{i\delta(k)}e^{i\delta'(k)}e^{-i(m-1)k}, \quad \text{(D5)}$$

for $m = 1, \dots, M$, with boundary values

$$y_0'(k) = i\frac{\sinh(2h_1)\cosh K_1^\star}{\sinh\gamma(k)}y_1'(k),$$

$$y_{2M+1}'(k) = i\frac{\sinh(2h_1)\cosh K_1^\star}{\sinh\gamma(k)}y_{2M}'(k). \quad \text{(D6)}$$

The allowed momenta k are the same as for the V symmetrization and are found as the solutions of Eq. (31). It is convenient to single out from the spectral sum the contributions from the two imaginary wave numbers and write

$$e^{-F(N,M)} = T(iv_1) + T(iv_2) + \text{(real modes)}, \quad \text{(D7)}$$

where

$$T(iv) = (N')^2(iv)\left[\frac{\sinh(2h_1)\cosh K_1^\star}{\sinh\gamma(iv)}\right]^2 e^{-N\gamma(iv)}$$
$$\times \left[se^{2i\delta'(iv)}e^{-2v} + 2e^{i\delta'(iv)}e^{-(M+1)v} + se^{-2Mv}\right]. \quad \text{(D8)}$$

Since $\gamma(k_1) < \gamma(k_2) < \gamma(k_3) \dots < \gamma(k_M)$, contributions from the real wave number decay faster than those from imaginary modes and can therefore be neglected in the regime of our interest. In the limit $M \to \infty$ the sum of imaginary terms cancel out because the two imaginary solutions $k_1 = iv_1$ and $k_2 = iv_2$ are asymptotically degenerate and have the opposite parity number s [defined by Eq. (31)]. We expand $T(iv_i)$ around iv_0 for large M at fixed $N \gg M$ and keep the leading terms in M. From Eqs. (27) and (35), we have

$$\gamma(iv_i) \simeq \gamma(iv_0) + s/(2\xi_\parallel) \quad (i = 1, 2), \quad \text{(D9)}$$

and thus

$$e^{-N\gamma(iv_i)} \simeq e^{-N\gamma(iv_0)}[1 + Ns/(2\xi_\parallel)] \quad (i = 1, 2), \quad \text{(D10)}$$

where $s = +1$ for v_1 and $s = -1$ for v_2 and $\xi_\parallel$ is given by Eq. (48). In the limit $M \to \infty$, the normalization constant takes the following form:

$$(N')^2(iv) \simeq \frac{w^2 - 1}{2e^{2i\delta'(iv_0)}}$$
$$- 2sw^{-1}e^{i\delta'(iv_0)}\left[\frac{w^2 - 1}{2e^{2i\delta'(iv_0)}}\right]^2 Me^{-Mv_0}, \quad \text{(D11)}$$

and the prefactor multiplying the square brackets in Eq. (D8) can be factorized:

$$\frac{\sinh(2h_1)\cosh K_1^\star}{\sinh\gamma(iv_0)} = w\sqrt{\frac{AB-1}{(Aw-1)(Bw-1)}}. \quad \text{(D12)}$$

Neglecting all terms of the order of e^{-Mv_0} and higher as subdominant with respect to Me^{-Mv_0} and using Eq. (C3), we find

$$T(iv_1) + T(iv_2)$$
$$\simeq -e^{-N\gamma(iv_0)-Mv_0}\frac{\sqrt{AB}(AB-1)w^2(w-w^{-1})^3}{(Aw-1)^2(Bw-1)^2}$$
$$\times \left\{N - M\frac{[(Aw-1)(Bw-1)(w-A^{-1})(w-B^{-1})]^{1/2}}{w^2-1}\right\}. \quad \text{(D13)}$$
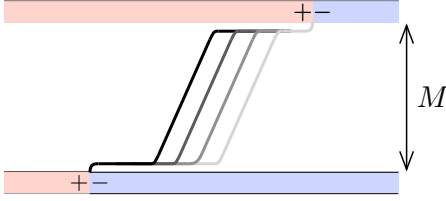
FIG. 13. Displacements of the inclined portion of the domain wall which do not alter the free energy.

The contact angle Θ can be identified by expressing Eq. (A8), which is an implicit equation for Θ, in the factorized form

$$\frac{\sqrt{(w-A)(w-B)(w-A^{-1})(w-B^{-1})}}{w^2-1} = \cot\Theta. \quad (D14)$$

The final result for the free energy $F(N,M)$ of the domain wall can be written as

$$e^{-F(N,M)} = (N - M\cot\Theta)\underbrace{\frac{(AB-1)(w^2-1)}{(Aw-1)(Bw-1)}e^{-N\gamma(iv_0)}}_{\text{horizontal}}$$

$$\times e^{-2\tau_p}e^{-Mv_0}, \quad (D15)$$

where

$$e^{-2\tau_p} = \frac{w\sqrt{AB}(w^2-1)^2}{(Aw-1)(Bw-1)}. \quad (D16)$$

Let us analyze the meaning of the various factors appearing in Eq. (D15). The quantity in parentheses is the entropic factor, which gives the number of ways in which it is possible to displace the inclined portion of the domain wall without altering the free-energy cost; see Fig. 13 for an illustration.

Additional calculations show that the contribution labeled "horizontal" is due to a flat portion of a domain wall pinned to the surface with fixed ends (lines AC and DB in in Fig. 10). Since $N\gamma(iv_0) = Nf_0$ [see Eq. (A6)] is the free energy of such domain wall with length N, the other factor must be the contribution from the end points (points A and B in in Fig. 10). For additional calculations we have considered a lattice with spins reversed between 1 and N at a bottom edge of the strip as shown in Fig. 12(b) to introduce a domain wall running parallel to the (1,0) axis. The free energy of such domain wall is given by Eq. (D1) but with $-\sigma_{M+1}^z$ replaced by $-\sigma_0^z$ and can be computed in the similar way as above. The final result reduces in the limit of $M \to \infty$ at fixed and large N to the expression labeled as "horizontal" in Eq. (D15). The interpretation of the remaining terms is now straightforward. Mv_0 is the excess free energy corresponding to the cost of replacing a piece of flat domain wall of length $M\cot\Theta$ (line CD in Fig. 10) by the inclined one. Thus we can write

$$Mv_0 = M\csc\Theta\,\tau(\Theta) - M\cot\Theta f_0, \quad (D17)$$

where $\tau(\Theta)$ is the angle-dependent surface tension at the wetting angle. This agrees with expression (A3) for $\mathcal{F}(\vartheta)$ from the free-energy considerations in Appendix A. Finally, τ_p in Eq. (D16) can be interpreted as a point tension (contributions from points C and D in Fig. 10).

As the wetting temperature T_w is approached, $v_0 = \ln w \searrow 0$ and therefore $\mathcal{F}(\Theta) = |\alpha(h_1)|M(T_w - T) + O[M(T_w -$

$T)^2]$, where the prefactor $\alpha(h_1)$ depends on the surface field. This reveals the finite-size scaling of Parry and Evans [23] with the scaling variable $M^{1/\beta_s}(T_w - T)$, where $\beta_s = 1$ is the Abraham result for the adsorption critical exponent [25]. The scaling Ansatz is based on the conjecture that $T_w - T_c(M) \propto M^{-(1/\beta_s)}$ for the shift of the critical temperature $T_c(M)$ in the asymmetric strip (or slab). Therefore pseudocoexistence and the associated asymptotic degeneracy only occur for the scaling variable $M(T_w - T) \gg 1$. This in turn guarantees that the Boltzmann weight $\tilde{\zeta} = \exp[-\mathcal{F}(\Theta)] \ll 1$ in this regime.

APPENDIX E: THE SURFACE STATES AND EDGE MAGNETIZATION

Here we outline calculations of $\langle o|\sigma_1^x|o\rangle$ and $\langle e|\sigma_M^x|e\rangle$ and of the edge magnetization for equal and opposing surface fields. First, we express the spin operators in terms of spinors. From Eqs (22) and (23) we find $\sigma_1^x = i\Gamma_{-1}\Gamma_0\Gamma_1$ with $\Gamma_{-1} = X_0 + X_0^\dagger$ and $\sigma_M^x = -i\Gamma_{2M}\Gamma_{2M+1}\mathcal{P}_{M+1}(X_0 - X_0^\dagger)$. $\mathcal{P}_{M+1}$ is the parity operator given by Eq. (23) with $m = M + 1$. We need to know the action of $\mathcal{P}_{M+1}$ on the vacuum and the excited states. It can be shown that $\mathcal{P}_{M+1}|\Phi_\infty\rangle = -|\Phi_\infty\rangle$ and $\mathcal{P}_M X^\dagger(k_1)\ldots X^\dagger(k_n)|\Phi_\infty\rangle = (-1)^{n+1}X^\dagger(k_1)\ldots X^\dagger(k_n)|\Phi_\infty\rangle$. Using definitions of the surfaces states [Eq. (53)], we find

$$\langle o|\sigma_1^x|o\rangle = -\tfrac{1}{2}(A_1 + A_2 - B_{12} - B_{21}),$$

$$\langle e|\sigma_M^x|e\rangle = \tfrac{1}{2}(\tilde{A}_1 + \tilde{A}_2 + \tilde{B}_{12} + \tilde{B}_{21}), \quad (E1)$$

where for $i = 1, 2$

$$A_i = \langle \Phi_\infty|X(iv_i)i\Gamma_0\Gamma_1 X^\dagger(iv_i)|\Phi_\infty\rangle$$

$$\tilde{A}_i = \langle \Phi_\infty|X(iv_i)i\Gamma_{2M}\Gamma_{2M+1}X^\dagger(iv_i)|\Phi_\infty\rangle, \quad (E2)$$

and for $i, j = 1, 2$ and $i \neq j$

$$B_{ij} = \langle \Phi_\infty|X(iv_i)i\Gamma_0\Gamma_1 X^\dagger(iv_j)|\Phi_\infty\rangle$$

$$\tilde{B}_{ij} = \langle \Phi_\infty|X(iv_i)i\Gamma_{2M}\Gamma_{2M+1}X^\dagger(iv_j)|\Phi_\infty\rangle. \quad (E3)$$

In order to evaluate these form factors, we employ the relation between spinors and fermionic operators,

$$\Gamma_m = \sum_{k \in \Omega_M} N(k)[y_m(k)(X_k)^\dagger + (y_m)^*(k)X_k], \quad (E4)$$

which corresponds to the inversion of Eq. (25). This gives

$$A_i = -iN^2(iv_i)y_1(iv_i)y_0^*(iv_i) + i\sum_{k \neq i} N^2(k)y_1(k)y_0^*(k)$$

$$\tilde{A}_i = -iN^2(iv_i)y_1(iv_i)y_0^*(iv_i) - i\sum_{k \neq i} N^2(k)y_1^*(k)y_0(k), \quad (E5)$$

for $i, j = 1, 2$ and

$$B_{ij} = iN(iv_i)N(iv_j)[y_0(iv_i)y_1^*(iv_j) - y_0^*(iv_j)y_1(iv_i)]$$

$$\tilde{B}_{ij} = iN(iv_i)N(iv_j)[y_1(iv_i)y_0^*(iv_j) - y_1^*(iv_j)y_0(iv_i)], \quad (E6)$$

for $i, j = 1, 2$ and $i \neq j$, where we have used the reflection symmetry [Eq. (34)] to express the eigenvectors y_{2M} and y_{2M+1} in terms of $y_0(k)$ and $y_1(k)$; the latter ones are given in Eq. (33).

Now we take the limit $M \to \infty$ in which $v_1, v_2 \to v_0$. In this limit the contributions from imaginary wave numbers

cancel each other in A_i and $\tilde{A}_i$ and we have

$$
A_1 = A_2 = \tilde{A}_1 = \tilde{A}_2 = 2\sqrt{\frac{AB}{(A-w)(B-w)}}
$$

$$
\times \lim_{M\to\infty} \sum_{k\in\text{real}} N^2(k)[\cos\delta^*(k) - \cos\delta(k)]. \quad \text{(E7)}
$$

In order to calculate B_{ij} and $\tilde{B}_{ij}$, we use the quantization condition [Eq. (31)] and eliminate $e^{i\delta}$ from the eigenvectors $y_0(iv_i)$ and $y_1(iv_i)$. Then we take the limit of $M \to \infty$ to find

$$
B_{ij} = -\tilde{B}_{ij} = -2N^2(iv_0)\sqrt{\frac{AB}{(A-w)(B-w)}}e^{-i\delta^*(iv_0)}
$$

$$
= \frac{w - w^{-1}}{\sqrt{(A^{-1}-w)(B^{-1}-w)}}. \quad \text{(E8)}
$$

The second line in the above equation is obtained using the asymptotic form of the normalization constant:

$$
N^{-2}(iv_0)e^{i\delta^*(iv_0)} = \frac{B}{B-w}e^{i\delta^*(iv_0)} + \frac{A}{A-w}e^{-i\delta^*(iv_0)}
$$

$$
+ \frac{1}{w^2-1}[e^{i\delta^*(iv_0)} + e^{-i\delta^*(iv_0)}]. \quad \text{(E9)}
$$

Bringing together all contributions and taking the limit $M \to \infty$ of the sum over the real wave numbers [51], we finally obtain:

$$
\langle o|\sigma_1^x|o\rangle = \frac{w - w^{-1}}{\sqrt{(A^{-1}-w)(B^{-1}-w)}} - \sqrt{\frac{AB}{(A-w)(B-w)}}
$$

$$
\times \int_{-\pi}^{\pi} \frac{dk}{2\pi}[\cos\delta^*(k) - \cos\delta(k)], \quad \text{(E10)}
$$

and

$$
\langle e|\sigma_M^x|e\rangle = -\frac{w - w^{-1}}{\sqrt{(A^{-1}-w)(B^{-1}-w)}} + \frac{\sqrt{AB}}{(A-w)(B-w)}
$$

$$
\times \int_{-\pi}^{\pi} \frac{dk}{2\pi}[\cos\delta^*(k) - \cos\delta(k)]. \quad \text{(E11)}
$$

In order to demonstrate the relations (56), let us calculate the edge magnetization $\mathfrak{m}_e(\alpha, \beta)$, where $\alpha = \pm 1$ is the sign of spins at the bottom edge and $\beta = \pm 1$ is the sign of spins fixed by the top edge—they are fixed by the surface field h_1 and h_2, respectively. For the bottom edge we have

$$
\mathfrak{m}_e^b(\alpha, \beta) = \frac{\text{Tr}[V^L P_0(\alpha)\sigma_1^x P_{M+1}(\beta)]}{\text{Tr}[V^L P_0(\alpha)P_{M+1}(\beta)]}, \quad \text{(E12)}
$$

where the projection operators are as follows:

$$
P_0(\alpha) = \frac{\alpha}{2}[I + \alpha(X_0 + X_0^\dagger)]
$$

$$
P_{M+1}(\beta) = \frac{1}{2}[I + \beta(X_0^\dagger - X_0)\mathcal{P}_{M+1}]. \quad \text{(E13)}
$$

Proceeding just like in the calculations for the surface states, we find

$$
\mathfrak{m}_e^b(+, -) = -\mathfrak{m}_e^b(-, +) = \langle\phi_\infty|X(iv_1)i\Gamma_0\Gamma_1 X^\dagger(iv_1)|\phi_\infty\rangle
$$

$$
= \sqrt{\frac{AB}{(A-w)(B-w)}}
$$

$$
\times \int_{-\pi}^{\pi} \frac{dk}{2\pi}([\cos\delta^*(k) - \cos\delta(k)], \quad \text{(E14)}
$$

and

$$
\mathfrak{m}_e^b(+, +) = -\mathfrak{m}_e^b(-, -) = \langle\phi_\infty|i\Gamma_0\Gamma_1|\phi_\infty\rangle
$$

$$
= -\frac{w - w^{-1}}{\sqrt{(A^{-1}-w)(B^{-1}-w)}}
$$

$$
+ \sqrt{\frac{AB}{(A-w)(B-w)}}
$$

$$
\times \int_{-\pi}^{\pi} \frac{dk}{2\pi}[\cos\delta^*(k) - \cos\delta(k)]. \quad \text{(E15)}
$$

For the top edge we have

$$
\mathfrak{m}_e^t(\alpha, \beta) = \frac{\text{Tr}[V^L P_0(\alpha)\sigma_M^x P_{M+1}(\beta)]}{\text{Tr}[V^L P_0(\alpha)P_{M+1}(\beta)]}. \quad \text{(E16)}
$$

An analogous evaluation gives

$$
\mathfrak{m}_e^t(-, +) = -\mathfrak{m}_e^t(+, -)
$$

$$
= \langle\phi_\infty|X(iv_1)i\Gamma_{2M}\Gamma_{2M+1}X^\dagger(iv_1)|\phi_\infty\rangle
$$

$$
= \frac{\sqrt{AB}}{(A-w)(B-w)} \int_{-\pi}^{\pi} \frac{dk}{2\pi}[\cos\delta^*(k) - \cos\delta(k)]. \quad \text{(E17)}
$$

We can see that $\mathfrak{m}_e^t(-, +) = -\mathfrak{m}_e^b(-, +)$. On the other hand

$$
\mathfrak{m}_e^t(+, +) = -\mathfrak{m}_e^t(-, -) = \langle\phi_\infty|i\Gamma_{2M}\Gamma_{2M+1}|\phi_\infty\rangle
$$

$$
= -\frac{w - w^{-1}}{\sqrt{(A^{-1}-w)(B^{-1}-w)}}
$$

$$
+ \frac{\sqrt{AB}}{(A-w)(B-w)} \int_{-\pi}^{\pi} \frac{dk}{2\pi}[\cos\delta^*(k) - \cos\delta(k)], \quad \text{(E18)}
$$

thus

$$
\mathfrak{m}_e^t(\pm, \pm) = \mathfrak{m}_e^b(\pm, \pm) = \mathfrak{m}_e \quad \text{(E19)}
$$

Comparing results for the edge magnetization with expressions for the surface states expectation values Eqs. (E10) and (E11), we arrive at the relation (56).

APPENDIX F: SOLUTION OF THE DISCRETIZATION EQUATION

Here we show how the discretization equation [Eq. (31)] admits two nearly degenerate imaginary solutions; see Ref. [14] where it was originally found. In order to proceed we set $k = iv$ with positive v. The left-hand side is the exponential $\exp(-Mv)$. The right-hand side, $s\exp[i\delta(iv)]$ requires special care because of the branch cut exhibited by
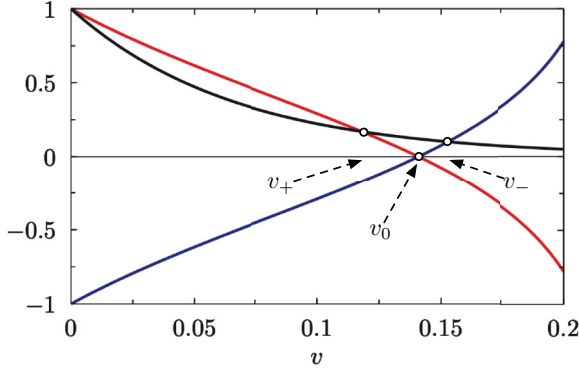
FIG. 14. Discretization equation for imaginary wave numbers. The left-hand side, $\exp(-Mv)$, is indicated with the solid black curve. The right-hand side, $s\exp[i\delta'(iv)]$, is shown with a solid red ($s = +1$) and blue line ($s = -1$). The corresponding solutions v_+ and v_- are shown. In this figure, $M = 15$ and the other parameters are the same as in Fig. 8.

the Onsager angle $\exp[i\delta'(k)]$. Since we are interested in the regime $T < T_c$, the branch is selected such that $\exp[i\delta'(0)] = -1$ because $\delta'(0) = \pi$. Therefore, the right-hand side of the discretization equation for a wave number along the imaginary axis is

$$e^{i\delta(iv)} = -\left(\frac{Ae^v - 1}{A - e^v}\frac{Be^v - 1}{B - e^v}\right)^{1/2}\frac{e^v - w}{we^v - 1}. \quad \text{(F1)}$$

Since we are interested in large values of M, the left-hand side is exponentially small; hence, the solution has to be found

in the closeness of the zero of the right-hand side. The zero occurs when the second factor of (F1) vanishes, which is at $v = \ln w \equiv v_0$. In view of the large-M asymptotic result we need, it is sufficient to perform a Taylor expansion of (F1) around $v = v_0$ of the second factor in (F1), which reads

$$\frac{e^v - w}{we^v - 1} = \frac{v - v_0}{w - w^{-1}} + O[(v - v_0)^2], \qquad v \to v_0. \quad \text{(F2)}$$

It is thus clear that the equation we need to solve is of the form

$$\exp(-Mv) = sQ(v - v_0) + O[(v - v_0)^2], \quad \text{(F3)}$$

where

$$Q = -\left(\frac{Aw - 1}{A - w}\frac{Bw - 1}{B - w}\right)^{1/2}\frac{1}{w - w^{-1}}, \quad \text{(F4)}$$

can be identified as the prefactor of $v - v_0$ appearing in (F3) evaluated at $v = v_0$. In Fig. 14 we show the left-hand side of the discretization equation together with the right-hand side with $s = +1$ and $s = -1$. The inclusion of additional terms beyond the linear one is necessary in order to work out an iterative solution beyond the leading order. By focusing on the leading-order term, the solution of (F3) is

$$v = v_0 + sQ^{-1}e^{-Mv_0} + O(e^{-2Mv_0}). \quad \text{(F5)}$$

It turns out that Q defined above is related to the quantity $\mathcal{A}$ defined in Eq. (36) via $Q = -\mathcal{A}^{-1}$. Neglecting the exponentially subleading terms of order $\exp(-2Mv_0)$, the solution is

$$v_s = v_0 - s\mathcal{A}e^{-Mv_0}, \quad \text{(F6)}$$

with $s = +1$ and $s = -1$. The solution closest to the real axis is the one with parity number $s = +1$.

[1] J. K. Perron, M. O. Kimball, K. P. Mooney, and F. M. Gasparini, Coupling and proximity effects in the superfluid transition in ^{4}He dots, Nat. Phys. **6**, 499 (2010).

[2] J. K. Perron, M. O. Kimball, and F. M. Gasparini, A review of giant correlation-length effects via proximity and weak-links coupling in a critical system: ^{4}He near the superfluid transition, Rep. Prog. Phys. **82**, 114501 (2019).

[3] M. E. Fisher, Proximity eases confinement, Nat. Phys. **6**, 483 (2010).

[4] D. B. Abraham, A. Maciołek, and O. Vasilyev, Emergent long-range couplings in arrays of fluid cells, Phys. Rev. Lett. **113**, 077204 (2014).

[5] D. B. Abraham, A. Maciołek, A. Squarcini, and O. Vasilyev, Action at a distance in classical uniaxial ferromagnetic arrays, Phys. Rev. E **96**, 042154 (2017).

[6] D. Bonn, J. Eggers, J. Indekeu, J. Meunier, and E. Rolley, Wetting and spreading, Rev. Mod. Phys. **81**, 739 (2009).

[7] M. E. Fisher and H. Nakanishi, Scaling theory for the criticality of fluids between plates, J. Chem. Phys. **75**, 5857 (1981).

[8] R. Peierls, On Ising's model of ferromagnetism, Math. Proc. Camb. Phil. Soc. **32**, 477 (1936).

[9] R. Griffiths, Peierls proof of spontaneous magnetization in a two-dimensional Ising ferromagnet, Phys. Rev. **136**, A437 (1964).

[10] M. Kac, *Mathematical Mechanisms in Phase Transitions* (Gordon & Breach, New York, 1966).

[11] D. B. Abraham, On the transfer matrix for the two-dimensional Ising model, Stud. Appl. Math. **50**, 71 (1971).

[12] D. B. Abraham and A. Martin-Löf, The transfer matrix for a pure phase in the two-dimensional Ising model, Commun. Math. Phys. **32**, 245 (1973).

[13] J. Stecki, A. Maciołek, and K. Olaussen, Magnetization profiles of the planar fluctuating interface in a $d = 2$ Ising strip, Phys. Rev. B **49**, 1092 (1994).

[14] A. Maciołek and S. Stecki, $d = 2$ Ising strips with two surface fields solved using the transfer-matrix method, Phys. Rev. B **54**, 1128 (1996).

[15] There is actually an *odd* numbers of such open Peierls contours but in the limit of large width the contribution due to the single contour is the one that dominates.

[16] V. Privman and M. E. Fisher, Finite-size effects at first-order transitions, J. Stat. Phys. **33**, 385 (1983).

[17] D. B. Abraham and L.-F. Ko, Exact derivation of the modified Young equation for partial wetting, Phys. Rev. Lett. **63**, 275 (1989).

[18] D. B. Abraham, F. Latrémolière, and P. J. Upton, Divergence of the point tension at wetting, Phys. Rev. Lett. **71**, 404 (1993).

[19] H. Au-Yang and M. E. Fisher, Wall effects in critical systems: Scaling in Ising model strips, Phys. Rev. B **21**, 3956 (1980).

[20] A. De Virgiliis, E. V. Albano, M. Müller, and K. Binder, Interfaces in the confined Ising system with competing surface fields, Physica A **352**, 477 (2005).

[21] E. Albano, K. Binder, D. W. Heermann, and W. Paul, Adsorption on stepped surfaces: A Monte Carlo simulation, Surf. Sci. **223**, 151 (1989).

[22] E. V. Albano, K. Binder, D. W. Heermann, and W. Paul, Critical wetting in the square Ising model with a boundary field, J. Stat. Phys. **61**, 161 (1990).

[23] A. O. Parry and R. Evans, Influence of wetting on phase equilibria: A novel mechanism for critical-point shifts in films, Phys. Rev. Lett. **64**, 439 (1990).

[24] A. O. Parry and R. Evans, Novel phase behaviour of a confined fluid or Ising magnet, Physica A **181**, 250 (1992).

[25] D. B. Abraham, Solvable model with a roughening transition for a planar Ising ferromagnet, Phys. Rev. Lett. **44**, 1165 (1980).

[26] K. Binder, R. Evans, D. P. Landau, and A. M. Ferrenberg, Interface localization transition in Ising films with competing walls: Ginzburg criterion and crossover scaling, Phys. Rev. E **53**, 5023 (1996).

[27] A. Milchev, M. Müller, K. Binder, and D. P. Landau, Interface localization-delocalization in a double wedge: A new universality class with strong fluctuations and anisotropic scaling, Phys. Rev. Lett. **90**, 136101 (2003).

[28] S. Kondrat, O. A. Vasilyev, and S. Dietrich, Probing interface localization-delocalization transitions by colloids, J. Phys.: Condens. Matter **30**, 414002 (2018).

[29] V. Privman and N. M. Švrakić, Finite-size scaling for the restricted solid-on-solid model of the two-dimensional wetting transition, Phys. Rev. B **37**, 3713 (1988).

[30] W. Selke, N. M. Švrakić, and P. J. Upton, Ising models with interfaces, defect lines, and walls, Z. Phys. B **89**, 231 (1992).

[31] D. B. Abraham, L.-F. Ko, and N. M. Švrakić, Transfer matrix spectrum for the finite-width Ising model with adjustable boundary conditions: Exact solution, J. Stat. Phys. **56**, 563 (1989).

[32] L. Tonks, The complete equation of state of one, two and three-dimensional gases of hard elastic spheres, Phys. Rev. **50**, 955 (1936).

[33] A. Robledo and J. S. Rowlinson, The distribution of hard rods on a line of finite length, Mol. Phys. **58**, 711 (1986).

[34] L. D. Landau and E. M. Lifshitz, *Statistical Physics, Part I* (Pergamon, Oxford, 1980).

[35] D. B. Abraham and P. Reed, Diagonal interface in the two-dimensional Ising ferromagnet, J. Phys. A: Math. Gen. **10**, L121 (1977).

[36] D. B. Abraham and P. J. Upton, Interface at general orientation in a two-dimensional Ising model, Phys. Rev. B **37**, 3835 (1988).

[37] L. Onsager, Crystal statistics. I. A two-dimensional model with an order-disorder transition, Phys. Rev. **65**, 117 (1944).

[38] C. J. Thompson, *Mathematical Statistical Mechanics* (Princeton University Press, Princeton, NJ, 2015).

[39] T. D. Schultz, D. C. Mattis, and E. H. Lieb, Two-dimensional Ising model as a soluble problem of many fermions, Rev. Mod. Phys. **36**, 856 (1964).

[40] B. Kaufman, Crystal statistics. II. Partition function evaluated by spinor analysis, Phys. Rev. **76**, 1232 (1949).

[41] B. M. McCoy and T. T. Wu, Theory of Toeplitz determinants and the spin correlations of the two-dimensional Ising model. IV, Phys. Rev. **162**, 436 (1967).

[42] B. M. McCoy, *The Two-dimensional Ising Model* (Harvard University Press, Cambridge, MA, 1973).

[43] A. Drzewiński, A. O. Parry, and K. Szota, Tests of nonuniversality and finite-size scaling for two-dimensional wetting with long-ranged forces, Phys. Rev. E **75**, 041110 (2007).

[44] Preliminary MC simulation results obtained by O. A. Vasilyev for a magnetic susceptibility of a 2D array of squares connected by strips with opposing surface fields $h_1 = -h_2$ show features signaling network ordering below the wetting temperature $T_w(h_1)$, which are consistent with our theory.

[45] T. D. Lee and C. N. Yang, Statistical theory of equations of state and phase transitions. II. Lattice gas and Ising model, Phys. Rev. **87**, 410 (1952).

[46] Equation (28) corresponds to the cosine theorem in hyperbolic geometry, which is nothing but Al-Kashi theorem in standard trigonometry provided the cosine is replaced by a hyperbolic cosine.

[47] A. Squarcini and A. Tinti, Droplet-mediated long-range interfacial correlations. Exact field theory for entropic repulsion effects, J. High Energy Phys. 03 (2023) 123.

[48] A. Squarcini and A. Tinti, Interfacially adsorbed bubbles determine the shape of droplets, SciPost Phys. **15**, 164 (2023).

[49] A. Squarcini and A. Tinti, Correlations and structure of interfaces in the Ising model: Theory and numerics, J. Stat. Mech. (2021) 083209.

[50] A. Squarcini and A. Tinti, Four-point interfacial correlation functions in two dimensions: Exact results from field theory and numerical simulations, J. Stat. Mech. (2021) 103205.

[51] Performing limit $M \to \infty$ of the sum over the real wave numbers k is not straightforward, because they are uniformly distributed between 0 and π.